nature protocols

https://doi.org/10.1038/s41596-025-01178-0

Protocol

Check for updates

Expansion and fluctuations-enhanced microscopy for nanoscale molecular profiling of cells and tissues

Dominik Kylies[1,2,9], Hannah S. Heil[3,8,9], Arturo G. Vesga[3,4], Mario Del Rosario[3,4], Maria Schwerk[1,2], Malte Kuehl[5,6], Milagros N. Wong[1,2,5,6], Victor G. Puelles[1,2,5,6,10] ✉ & Ricardo Henriques[3,4,7,10] ✉

Abstract

Advances in super-resolution microscopy enable the molecular profiling of cells and tissues at the nanoscale level, surpassing the diffraction limit of conventional light microscopy. However, super-resolution techniques typically require access to expensive specialized equipment and extensive training, limiting their broad applicability. Here we provide a detailed protocol for combining expansion microscopy with enhanced super-resolution radial fluctuations analysis to achieve nanoscale resolution using conventional microscopes. Expansion microscopy physically enlarges the sample, while enhanced super-resolution radial fluctuations computationally enhances the image resolution by analyzing fluorescence fluctuations over time. By combining both, we achieve images with a resolution of 25 nm in combination with diffraction-limited microscopes. Our step-by-step instructions include the expansion of cells and tissue samples, the optimization of multispectral microscopy parameters and the implementation of quality control metrics to minimize artifacts. We further cover the use of quantitative tools such as NanoJ-SQUIRREL, which enable the assessment of resolution improvements and image fidelity. We discuss key considerations for each stage, including sample preparation, image acquisition, computational processing and downstream analysis. Potential pitfalls and troubleshooting strategies are also addressed. This protocol can be used for imaging a variety of sample types with multiple fluorescent labels. With nanoscale spatial resolution and molecular specificity, expansion-enhanced super-resolution radial fluctuations microscopy provides a flexible, accessible approach for investigating cellular ultrastructure, protein localization and interaction networks, suitable for applications in cell biology, histopathology and biomedical research. The procedure requires 3–4 d to complete, involving ~7–9 h of total bench, imaging and processing time and only requires basic expertise in tissue handling, molecular and cell biology, and microscopy.

Key points

- The expansion-enhanced super-resolution radial fluctuations procedure covers molecular sample labeling, followed by the expansion pipeline (including anchoring, polymerization, digestion and expansion) and enhanced super-resolution radial fluctuations imaging (including mounting, imaging, computational image enhancement, image analysis and quality control).
- Alternative methods also combine the use of fluorescence-fluctuations detection algorithms with fourfold or tenfold expansion microscopy protocols, such as Magnify or the resource-intensive One microscopy. Expansion-enhanced super-resolution radial fluctuations is advantageous for imaging large-scale tissue samples such as clinical biopsies.

Key references

Kylies, D. et al. *Nat. Nanotechnol.* **18**, 336–342 (2023): https://doi.org/10.1038/s41565-023-01328-z

Laine, R. F. et al. *Nat. Methods* **20**, 1949–1956 (2023): https://doi.org/10.1038/s41592-023-02057-w

Culley, S. et al. *Nat. Methods* **15**, 263–266 (2018): https://doi.org/10.1038/nmeth.4605

A full list of affiliations appears at the end of the paper. ✉e-mail: vgpuelles@clin.au.dk; r.henriques@itqb.unl.pt

Introduction

Deciphering the intricate ultrastructure of cells is crucial for understanding cell biology and its implications for health and disease. Super-resolution microscopy (SRM) approaches enable molecular profiling at the nanoscale by surpassing the diffraction limit of light, a physical barrier limiting the resolution of conventional light microscopy systems to ~250–300 nm. Over the past decades, numerous SRM approaches have emerged, including structured illumination microscopy[1,2], stimulated emission depletion (STED)[3] and single-molecule localization microscopy[4] approaches such as stochastic optical reconstruction microscopy[5,6], among others[7]. Despite these groundbreaking advancements, the widespread adoption of SRM in biological laboratories and clinical pathology units has been hindered by several challenges. These include the requirement for costly specialized equipment, the need for extensive and specialized training and, in some cases, limitations in the availability of optimized fluorophores for multicolor imaging. Recent efforts have focused on developing alternative approaches that are reliable, reproducible, flexible and less reliant on expensive and specialized equipment, thereby increasing the accessibility and applicability of super-resolution imaging in diverse research settings.

One technology that fits these criteria is expansion microscopy (ExM)[8]. In ExM, biological specimens are embedded in a swellable hydrogel used to isotropically expand specimens in all three dimensions, achieving super-resolution with diffraction-limited microscopes (Box 1). The original ExM protocols achieved an approximately fourfold unidimensional isotropic expansion factor, allowing a lateral resolution of up to 70 nm in biological specimens in combination with diffraction-limited microscopes[8–10]. Since its implementation, other ExM protocols have been developed that enable even higher resolutions by enhancing the degrees of unidimensional expansion from fourfold to the range of 10–20-fold[11–14]. However, this comes at the cost of more complex handling procedures, a reduced field of view and low signal levels due to the dilution of fluorophore density[15]. As a result, most ExM applications currently rely on well-established fourfold expansion protocols, striking a balance between resolution improvement and practical usability. The successful application of ExM in the field of life sciences[16–19] and additional advances, including in the development of novel anchoring strategies[14,20,21] and adaptations for specific sample requirements[22–25], further aided in establishing ExM as a widely accepted and flexible methodology for the ultrastructural profiling of biological specimens.

An alternative approach to achieving super-resolution without specialized equipment is fluctuation analysis-based computational image enhancement. Among the various techniques available[26–29], super-resolution radial fluctuations (SRRF)[30], and its recently published enhanced version eSRRF[31], have emerged as versatile and widely adopted methods for live-cell SRM. The popularity of (e)SRRF is evident from its extensive use within the scientific community[32–38], as it can be applied across various microscopy setups using commonly employed fluorescent molecular probes[39]. (e)SRRF enhances the resolution by analyzing a timelapse image series through a stepwise process that measures local radial symmetries and temporal fluctuations over time. This process ultimately results in reconstructing a single super-resolution image with an improved signal-to-noise ratio and a resolution range of 60–150 nm (ref. 30) (Box 2), making it compatible with most conventional fluorescence microscopes.

By redefining some of the fundamental reconstruction principles, the new eSRRF implementation succeeds in improving image fidelity and resolution and even extends to 3D super-resolution in combination with multifocal detection modalities. eSRRF also incorporates an automated parameter optimization feature based on quantitative image quality metrics for image quality and resolution, enhancing user-friendliness and reproducibility[31].

In this context, we recently developed a novel modular super-resolution pipeline ‘expansion-enhanced super-resolution radial fluctuations’ (ExSRRF)[40] that combines the principles of ExM and fluctuation-based image processing. Here, we present a detailed step-by-step protocol to enable new users without prior experience to quickly adopt this technology for nanoscale profiling. We provide an overview of the principal stages and experimental timeline (Fig. 1), along with detailed instructions. These step-by-step instructions

BOX 1

Expansion microscopy

The first reported protocol for ExM was established by the Boyden laboratory in 2015, leveraging the well-established properties of certain acrylate-based hydrogels to isotropically swell in contact with deionized water[8]. The ExM approach was proposed as a means of enhancing the effective resolution in microscopy by increasing the size of biological samples, utilizing a specific gel chemistry resulting in a fourfold increase in sample size. The original ExM protocol required a customized label, containing a methacryloyl group to engage in free radical polymerization, a DNA-oligonucleotide capable of hybridizing with a complementary sequence linked to an affinity tag and a chemical fluorophore for visualization purposes. Subsequent protocols replaced this anchoring and labeling strategy with a direct protein anchoring to the gel[9,73], eliminating the need for customized fluorophores and enabling ExM to be adopted by a broad community. Therefore, in its most widely adopted forms, in ExM, a fluorescently labeled specimen (1) generally undergoes an anchoring treatment (2) to facilitate attachment of biomolecules to the hydrogel matrix after hydrogel embedding (3), followed by homogenization (4) and incubation in deionized water resulting in isotropic sample expansion (5). It is important to highlight that, for the sake of illustration, the sizes of the hydrogel mesh and of the cells are not true to scale. Of note, in this rapidly evolving field, in recent years, several alternative developments have been made, expanding upon the widely used fourfold protocols of ExM. These include achieving higher degrees of expansion using iterative expansion[11] or alternative gel chemistries that allow for up to tenfold expansion in a single round of expansion[12,13], as well as exploring novel protein anchoring strategies (including novel chemical[14] and physical[74]) and alternative gel chemistries to further enhance stability and nanoscale precision[22].

One critical aspect of ensuring both the quality control and the quantitative reliability of the ExM approach is the accurate assessment of the expansion factor. While measuring the increase in gel size after expansion serves as an important control step—helping verify that the gelation and expansion procedures have been executed properly—this method alone is not a reliable indicator of the effective expansion factor at the sample level. The overall gel size may expand uniformly, but local variations in the sample can result in different effective expansion factors for biological structures. To more precisely estimate the effective expansion factor, it is necessary to measure features within the sample that have a well-characterized and narrow size distribution, such as cell sizes or nuclear diameters (as outlined by Heil et al. in their Platelet ExM study[75]). However, even this method is limited by biological variability. For truly accurate measurement of the expansion factor, a direct comparison of pre- and post-expansion views of the same structure is ideal. This allows for direct analysis of the dimensional changes[8,41]. Alternatively, well-defined molecular or synthetic structures, such as fluorescent beads or nanostructured grids, can serve as internal 'rulers', offering a reliable, standardized reference for assessing how much the sample has expanded[76–79]. These approaches enable a more quantitative and precise determination of the actual expansion factor, ensuring more robust and reproducible results in ExM experiments.

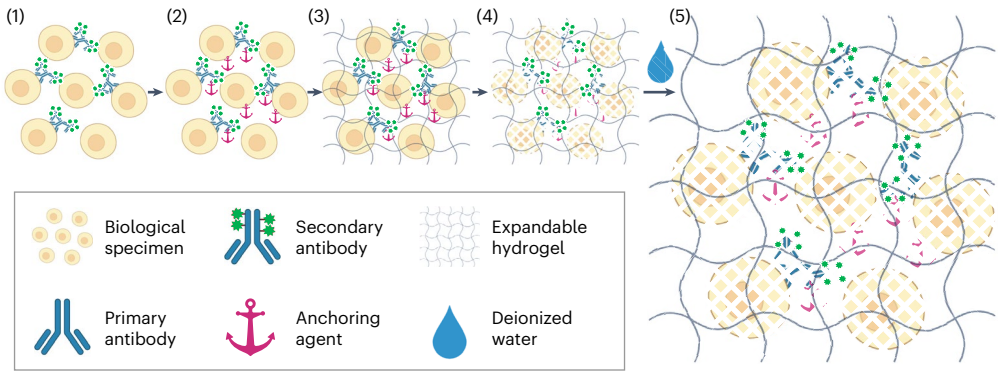

highlight challenges and provide concepts for troubleshooting, quality control and image analysis. While this protocol aims to help users adopt and optimize the ExSRRF workflow, many of the aspects discussed in this protocol will also apply to immunofluorescence microscopy, ExM and fluorescence fluctuation detection algorithms in general.

Development of the procedure

The ExSRRF method was developed as a versatile and widely applicable pipeline for nanoscale profiling of biological specimens. To ensure broad accessibility, we built upon the most

BOX 2

The eSRRF principle

SRRF was pioneered by the Henriques laboratory in 2016—recently updated to eSRRF—as a novel tool to enable live-cell super-resolution imaging in combination with conventional microscopes to overcome several limitations of SRM in this particular field[30,31]. While single-molecule localization microscopy techniques such as stochastic optical reconstruction microscopy rely on the induction of photoswitching kinetics of the fluorophores to keep most emitters in an off-state and only detect and localize the signals of subsets of individual well-separated molecules, eSRRF does not require single-molecule blinking.

The eSRRF method, visualized in the figure on the right, generates super-resolved images by relying on intensity fluctuations, even in cases with dense overlapping emitter signals. Using a short sequence of images (raw stack, top left), eSRRF surpasses diffraction-limited WF resolution (top middle) and reveals the underlying ultrastructure (eSRRF/SRRF, right; scale bars, 2 µm). Compared with SRRF, eSRRF achieves superior reconstruction fidelity, as quantified by resolution-scaled error (RSE: 13.3 for eSRRF versus 19.1 for SRRF).

The approach takes advantage of two basic principles: that fluorescent molecules emit radially, and their intensity fluctuations are temporally correlated, unlike background noise. To pick up the radial emission patterns in each image in the time stack, eSRRF magnifies pixels (magnification $M = 5$) and calculates intensity gradients in both the x and y directions (G_x, red; G_y, blue). Using a distance-dependent weighting map (Gaussian profile, $R = 1.5$, white arrow), these gradients are converted into a radial gradient convergence (RGC) map, which highlights fluorescent molecule positions as points of high RGC. The temporal analysis capabilities of eSRRF have been substantially refined to accommodate diverse imaging scenarios. The temporal average projection (AVG) stands as the most reliable approach, demonstrating superior robustness against artifacts when dealing with high-density molecular environments. This method effectively processes data across varying experimental conditions while maintaining reconstruction fidelity. For scenarios where fluorophores exhibit pronounced intensity fluctuations and are sparsely distributed, higher-order correlation analyses through VAR and TAC2 can achieve enhanced resolution. However, these approaches demand careful consideration, as they are particularly susceptible to noise and can generate significant artifacts if the experimental conditions are suboptimal. Finally, the sensitivity parameter (S) controls PSF sharpening power in eSRRF. More in-depth information can be found in the eSRRF publication[31].

Fluctuation analysis techniques such as eSRRF demonstrate significant nonlinearity, demanding precise parameter tuning to minimize reconstruction artifacts when handling imaging

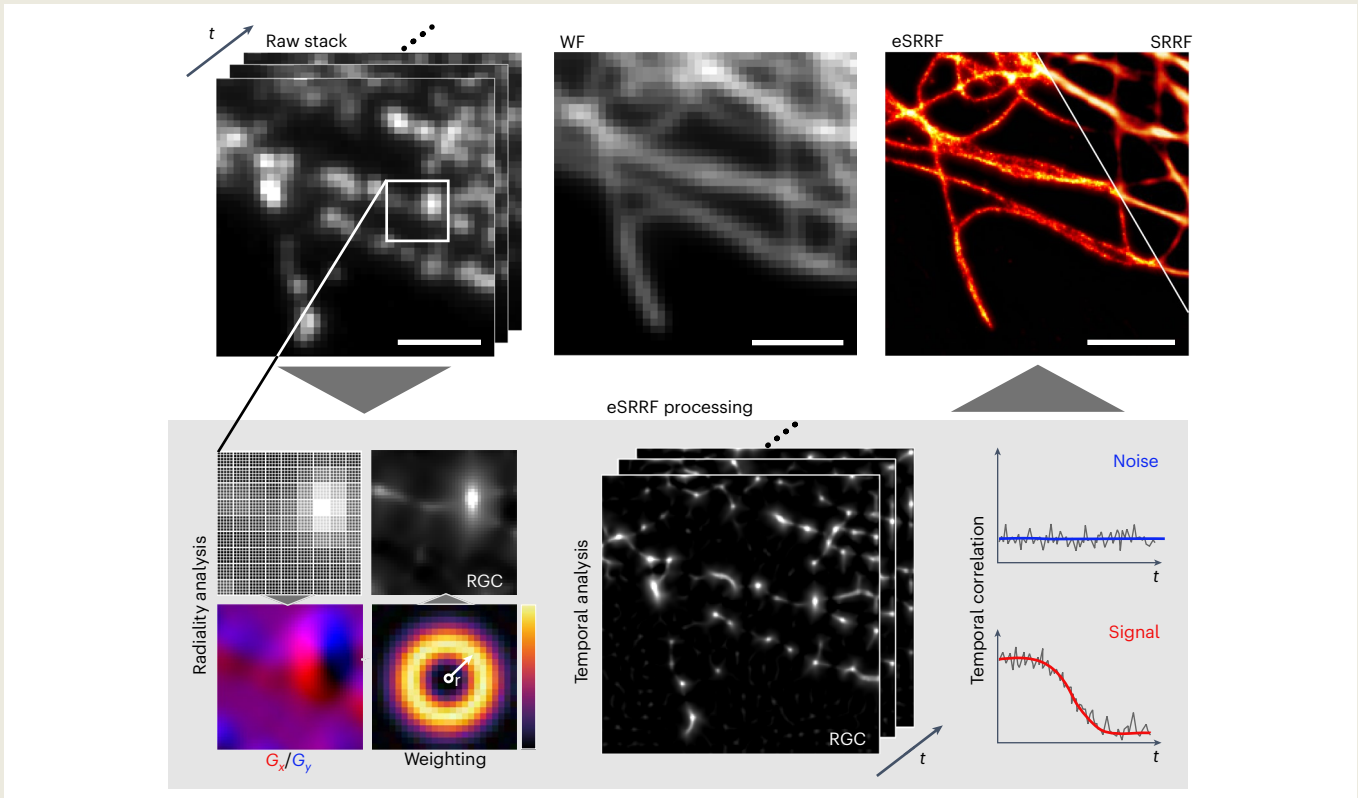

(continued from previous page)

data from a broad spectrum of microscopy platforms[46]. While the signal nonlinearity introduced by the fluctuation analysis prevents quantitative comparison of signal levels, spatial signal patterns or distributions can be assessed. To avoid reconstruction artifacts, the implementation of stringent quality control protocols, anchored in quantitative image quality metrics, is imperative within this framework. Ideally, a super-resolved image reconstruction allows to achieve the best compromise between both image resolution and image fidelity. Both measures can be described by quantitative metrics. Image resolution is estimated based on FRC[80] or decorrelation analysis[81]. To assess image fidelity, local errors introduced by image processing can be charted in an error map or quantified by the global metric as the RSP coefficient[45]. This allows for example to quantify the image fidelity improvement. In eSRRF, this compromise is formulated in the QnR factor based on which parameter settings are optimized[31].

commonly used fourfold ExM protocols[8–10] combined with conventional widefield (WF) microscopes[40], which are among the most readily available fluorescence microscopes in life science laboratories. ExM inherently reduces the fluorophore density and overall brightness[9], and is incompatible with commonly used fluorescence-protective mounting media. To overcome these limitations and further enhance resolution, we proposed integrating ExM with (e)SRRF imaging. Fluctuation-based image enhancement techniques such as (e)SRRF do not require high laser intensities, specialized photoswitching buffers or dedicated microscopes, making them well-suited for ExM.

The versatility and applicability of the ExSRRF method was demonstrated and validated in a broad range of biological scenarios, tissue types and species in both clinical and experimental samples. Examples of its application include neoplastic, neurodegenerative, ischemic and autoinflammatory diseases and scenarios. Of note, ExSRRF was successfully applied even in challenging tissue types such as placenta tissue and bone marrow. Furthermore, as a demonstration of clinical translation and diagnostic applicability, it was demonstrated that ExSRRF can detect diagnostic and quantify ultrastructural patterns of disease in human clinical biopsies that would otherwise require electron microscopy to be detected.

The image processing of expanded specimens was originally based on the SRRF algorithm[40], whereas the eSRRF algorithm described here provides an improved framework with higher resolution and fidelity, leveraging the same fluctuations-based principles[31].

Overview of the procedure

The ExSRRF pipeline consists of a 12-stage procedure where the user starts with the molecular labeling of specimens, followed by the expansion pipeline (pre-expansion imaging, anchoring, polymerization, digestion and expansion) and then the eSRRF (mounting, post-expansion imaging, pre-processing quality control, computational image enhancement, post-processing quality control and image analysis). It is noteworthy that in this protocol we focus primarily on describing the ExSRRF pipeline in combination with indirect immunofluorescence as a molecular labeling approach for proteins, which are among one of the most widely targeted classes of biomolecules in ExM and SRM for super-resolved imaging. In addition, we also provide information on how to combine ExSRRF with RNAscope-based mRNA detection, one example of a widely adopted, robust and commercially available platform for mRNA detection in formalin-fixed paraffin-embedded (FFPE) samples. In this context, it is noteworthy that a number of other strategies for combining ExM with fluorescence in situ hybridization (FISH) have been described that, in principle, are therefore also applicable in the context of ExSRRF, for example, ExFISH[21], Magnify[14] or ChromExM[17]. It has to be highlighted that many of these protocols require either additional anchoring steps, modifications to the hydrogel chemistry or both[14,17,21]. In this rapidly growing field, novel protocols for combining ExM with additional classes of biomolecules may emerge in the future. We therefore here chose to focus on providing an easy to implement strategy for the detection of proteins and mRNA that requires minimal adjustment in combination with the most widely adopted ExM protocol variants[9,10]. The individual stages of the ExSRRF pipeline are described in more detail below.

Of note, since previous protocols on ExM workflows have been published[41–44], within this protocol we chose to primarily focus on the integration of the expansion workflow into the combined approach and on thoroughly explaining the (e)SRRF workflow in combination with

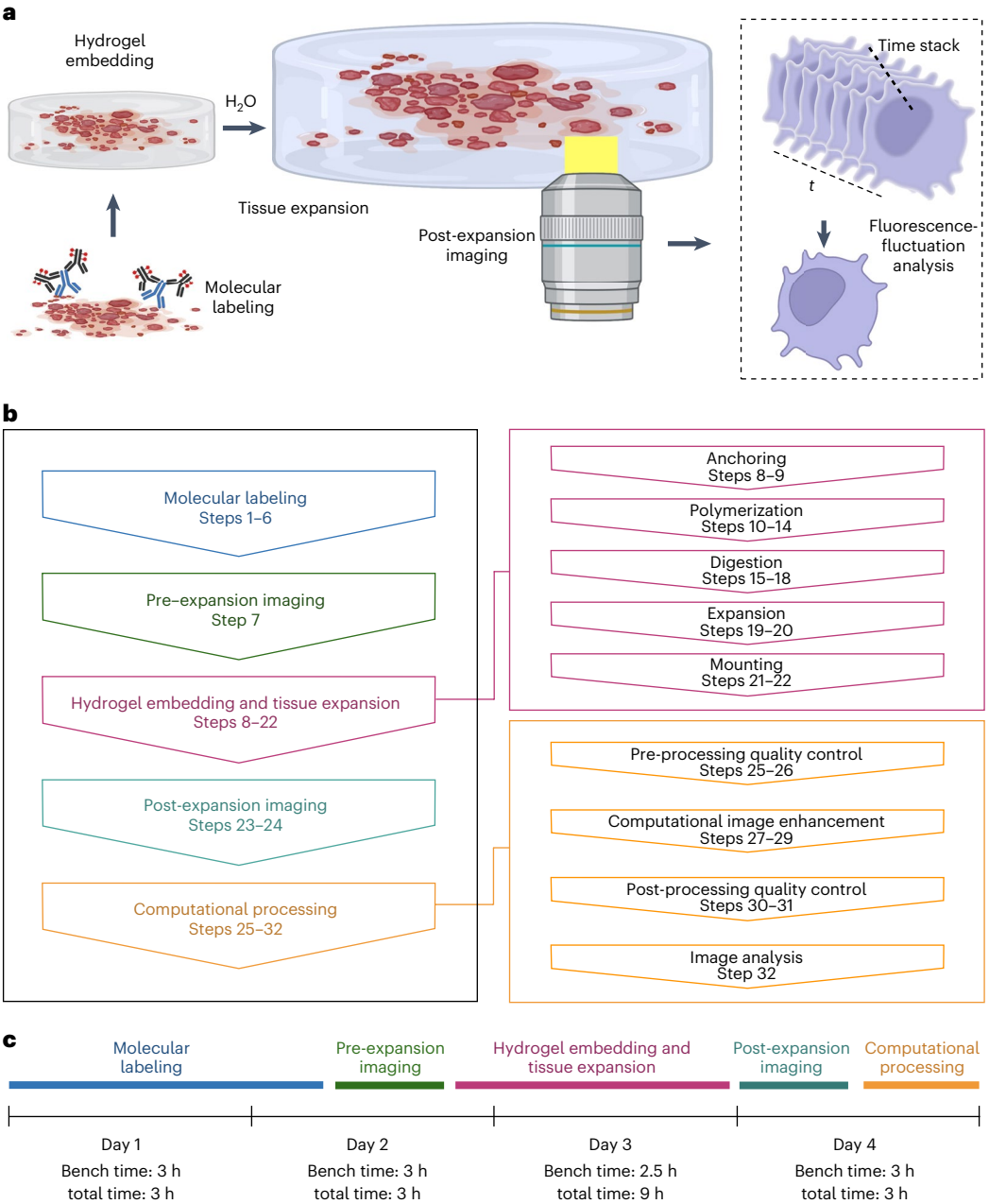

Fig. 1 | Overview and timeline of the expansion and fluctuations-enhanced microscopy workflow. a, Graphical overview of the general workflow. After molecular labeling, tissue specimens are embedded in hydrogel and expanded, followed by a time-lapse image acquisition and computational reconstruction using the eSRRF algorithm, resulting in the final super-resolution image. **b**, A schematic overview of the individual steps of the workflow **c**, Experimental timeline of the workflow including bench time and total experimental time per day.

sample expansion. Therefore, in the main protocol we only provide a brief overview over the labeling and tissue expansion stages. To ensure that users without previous experience in sample expansion can fully adopt the protocol without relying on external resources, we have incorporated a comprehensive protocol providing further details, including indications of hazardous risks, critical steps, tips and additional figures to better illustrate key aspects into Supplementary Note 2.

Molecular labeling of specimen (Steps 1–6)
Molecular labeling of biological specimen is the first stage and a critical step to achieving high-quality image data. Here, we describe an immunostaining protocol optimized for the fluorescent visualization of proteins within clinical and experimental FFPE tissues. However, alternative labeling protocols, including alternative immunolabeling protocols or fluorescent labeling of RNA may be applicable as well[9,10,21,40].

Pre-expansion imaging (Step 7)
Pre-expansion imaging is crucial in the workflow, serving as a key quality control step and forming the basis for correlative comparisons between pre-expansion and ExSRRF images. Inspecting tissue overviews before expansion helps identify potential artifacts, such as large-scale tissue distortions and ruptures. Additionally, these overviews provide a broad spatial context, help identify regions of interest and assist in accurately assessing biological distances, which can be challenging in expanded specimens.

Anchoring (Steps 8–9)
During the anchoring stage, the sample structure is linked to an anchoring agent, allowing biomolecules to attach to the acrylamide-based hydrogel for subsequent even expansion of the whole specimen. This section provides detailed information on the application of a frequently used and robust anchoring agent for protein targets: succinimidyl ester of 6-((acryloyl)amino) hexanoic acid, often simply referred to as 'acryloyl-X'. Acryloyl-X integrates into the gel matrix via its acrylate group and binds to the primary amines of proteins through its succinimidyl ester group, thereby covalently attaching proteins and fluorescently labeled antibodies to the gel[9]. Furthermore, in the troubleshooting section, we discuss alternative agents for protein anchoring. It is noteworthy, that different types of biomolecules may require additional anchoring strategies. For example, for the attachment of mRNA to the hydrogel, an anchoring strategy called 'Label X' has been described[21]. Of note, we found that for some particular RNAscope-based FISH kits, such as the RNAscope Multiplex Fluorescent kit, no additional anchoring step other than acryloyl-X is required. As the OPAL dyes used in RNAscope covalently bind to neighboring tissue proteins, there is no need for an additional mRNA anchoring step[40].

Polymerization (Steps 10–14)
During the polymerization stage, the tissue specimen is transformed into a tissue–hydrogel hybrid with the ability to expand. After the anchoring treatment, the tissue specimen is initially immersed in an activated monomer gelling solution, allowing the hydrogel monomers to evenly penetrate the tissue specimen. Since polymerization is a heat-dependent reaction, this penetration step is carried out at 4 °C to avoid premature polymerization. After completing the monomer penetration, a gelling chamber is assembled around the tissue specimen to provide an adequate gel size and thickness that can be consistently reproduced across multiple batches. The specimen is then moved to a humidified incubator at 37 °C allowing the monomers to polymerize into a solid hydrogel.

Digestion (Steps 15–18)
The digestion stage is essential for achieving artifact- and distortion-free tissue expansion by reducing and homogenizing tissue resistance. Inadequate digestion can restrict the maximum expansion factor attained and often leads to distortions or ruptures during the expansion process.

Tissue expansion (Steps 19–20)
After digestion, the specimen is removed from the slide and transferred to a container for incubation in double-deionized water (ddH_2O), which results in uniform tissue expansion.

Sample mounting (Steps 21–22)
It is crucial to mount and immobilize the expanded specimen correctly to obtain artifact-free images. Before mounting the specimen on glass-bottom chamber slides, a coating with

poly-D-lysine is applied to promote adhesion and minimize lateral movement during image acquisition. Following the coating, expanded specimens are placed on the poly-D-lysine-coated slides and then transferred to the microscope for image acquisition.

Post-expansion imaging (Steps 23–24)
The post-expansion imaging stage is a unique part of the ExSRRF workflow that differs considerably from most imaging protocols in conventional and expanded specimens. While for standard ExM procedures, single images are obtained[8], ExSRRF requires the acquisition of a fast temporal image series of the region of interest (ROI) to record fluctuations in the fluorescence signal and acquire imaging data that allows for subsequent eSRRF processing[31]. ExSRRF imaging of the expanded specimen is compatible with a wide range of microscopy systems, including light-emitting diode (LED)- and laser-illuminated WF and laser-scanning confocal microscopes. To achieve optimal results, imaging should be performed on an inverted microscope with a high-numerical-aperture (NA) immersion objective. This system must have sufficient acquisition speed of 20 Hz or more to capture fluorescence fluctuations and minimize movement artifacts, which can degrade the final image quality and resolution. This consideration is particularly important when capturing multichannel images. While WF systems have proven immensely powerful for thin tissue sections with ExSRRF, the use of confocal microscopy, and particularly spinning-disc confocal systems, is advised for thicker samples to exclude out of focus signal by optical sectioning.

Pre-processing quality control and corrections (Steps 25–26)
Before processing the images using eSRRF, it is crucial to perform pre-processing quality control. This should ideally start during image acquisition. The main purpose of this step is to identify major artifacts, such as lateral movement within the timelapse image series, which could affect the final ExSRRF image quality. We will also cover computational pre-processing steps to quantify and address these movement artifacts.

Computational image enhancement (Steps 27–29)
After capturing a series of timelapse images of the enlarged specimen, we proceed with computational processing using the eSRRF algorithm. The key factors to consider at this stage include fine-tuning the eSRRF parameter settings to achieve the best image quality, implementing various strategies to minimize processing time and handling multichannel image processing.

Post-processing quality control (Steps 30–31)
Post-processing quality control involves identifying and excluding artifacts through comparison of ExSRRF images to conventional images within the same regions, as well as the computational detection of processing artifacts through super-resolution quality control algorithms (for example, SQUIRREL[45]).

Image analysis (Step 32)
Ultimately, we discuss various strategies for automated segmentation and automated image analysis to obtain quantifiable molecular morphometrics at a nanoscale ('nanometrics'), ranging from the development and application of customized tools to the applicability of open-source algorithms and strategies.

Applications of the procedure

The combined expansion and fluctuation analysis-enhanced microscopy is a versatile tool that can be applied in various life science applications due to its modular approach. This technique has been proven to be adaptable to numerous experimental and clinical scenarios, including the study of neoplastic, neurodegenerative, inflammatory, genetic and ischemic diseases. Additionally, it has been demonstrated to be compatible with detecting proteins using immunofluorescence and mRNA through RNAscope-based FISH. This dual capability enables comprehensive analysis of biological samples, enabling researchers to explore the relationships between gene expression and protein localization in a single experiment[40].

Alternative methods

The adoption of ExM as a widely accessible SRM tool has spurred interest in combining it with other optical and computational SRM methods, leading to novel SRM approaches. A key focus has been integrating ExM with fluorescence fluctuations-based SRM algorithms, which improve resolution without requiring specialized setups and equipment. So far, several of these combined workflows leverage fluorescence-fluctuations detection algorithms[26,31,39,46] with both fourfold ExM[37,40] and tenfold ExM[14,36] protocols.

Each of these approaches addresses specific requirements posed by the sample type, desired resolution and experimental goals. For example, combining super-resolution optical fluctuation imaging with Magnify has been shown to provide enhanced resolution with a mechanically sturdy gel that retains nucleic acids, proteins, and lipids without needing a separate anchoring step, particularly for tenfold expansion[14].

A recent advancement in this field is the one-step nanoscale expansion (ONE) microscopy methodology[36], which achieves single-digit nanometer resolution through the synergistic combination of SRRF with advanced expansion protocols providing greater than fourfold expansion, specifically utilizing the X10-ExM protocol[12,41]. This methodology enables unprecedented structural visualization of individual proteins under optimized conditions.

The exceptional resolution capabilities of ONE microscopy stem from two key technical innovations. First, it employs advanced expansion protocols that achieve substantially higher expansion factors[41] compared with conventional ExM approaches[8,9], including the ExPath protocol[10] used in the ExSRRF methodology[40]. Second, the methodology incorporates extensive frame acquisition, collecting up to 4,000 frames per ROI for SRRF reconstruction, which stands in marked contrast to the 20–200 frames typically acquired in typical SRRF protocols.

While methods combining fluctuation-based super-resolution with tenfold expansion protocols demonstrate superior resolution performance, approaches utilizing fourfold expansion protocols, such as ExSRRF[40], maintain distinct practical advantages. These protocols excel in applications requiring preserved tissue context, such as intact clinical biopsies. Furthermore, the reduced frame count acquisition translates to decreased storage requirements and faster reconstruction times, making it particularly suitable for large-scale tissue analysis applications. The ExPath protocol, which we have extensively validated, remains particularly valuable for clinical FFPE sample analysis[10].

The selection between these methodological approaches necessitates careful consideration of multiple experimental parameters including, but not limited to, the specific sample characteristics, required resolution thresholds and the precise nature of the biological investigation. This understanding has profoundly influenced our protocol development strategy, ensuring adaptability across diverse experimental scenarios while maintaining rigorous scientific standards.

Limitations

General limitations and consideration in SRM

Many general considerations that apply to SRM also apply in the context of combined expansion and fluctuation analysis-enhanced microscopy. The nanoscale architecture of the specimen must be preserved sufficiently to allow for ultrastructural visualization. This includes correct sample preparation and optimizing fixation conditions for the imaging targets. To correctly label the structure of interest, the molecular labeling approach should ideally have a high affinity with little to no off-target effects. In addition, for a biological structure to be fully visualized, the target must be sufficiently spatially sampled with fluorophores, which means that the labeling density must be optimized. Here, post-expansion labeling approaches can benefit from the improved accessibility of targets due to protein decrowding[1]. Ultimately, the structure to be visualized must be within the resolution range of the SRM method[47].

Linkage error

Linkage error refers to the systematic offset between the location of the fluorescent probe as observed by fluorescence microscopy and the actual position of the target protein introduced by the labeling strategy. Indirect immunolabeling via primary/secondary antibody complexes

can amount to a spatial offset of 15–20 nm[48]. This offset's relevance can become increasingly important with SRM technologies whose high resolutions start approaching the size of labeling probes. Alternative strategies to potentially reduce linkage error in SRM and particularly in ExM include nanobody-based labeling approaches[49,50], labeling strategies based around genetic modifications of the specimen, including the expression of fluorescent proteins[9], self-labeling protein tags[20,51], grafting of peptide ligands[52,53] or in case of expansion-based methods post-expansion labeling[48]. Another aspect that must be considered here is the degree of labeling of each fluorescent tag. Indirect immunolabeling can result in a higher fluorescence signal simply because each secondary antibody usually carries two to five fluorescent markers, while smaller tags with degree of labeling close to one will result in lower signal levels[54].

Mechanical properties of the sample

One of the main potential sources of error in ExM are the substantial structural alterations during the sample preparation and expansion process. This manipulation of the sample during sample preparation can potentially lead to distortions or ruptures within the specimen, especially if not handled carefully. However, it is important to note that tissue preparation methods, including preparation protocols for other SRM methods, are also susceptible to distortions or ruptures due to factors such as fixation, embedding, sectioning, mounting, permeabilization and handling. The severity of these issues also depends on the sample's mechanical properties and homogeneity. Mechanically tougher samples, such as kidney tissue or bone marrow, may pose greater challenges in tissue expansion than mechanically less rigid and more homogeneous samples such as single-layered cell cultures[55–57]. Therefore, to optimize sample preparation for SRM and especially for ExSRRF, individual consideration of the sample properties may be necessary.

Distortions and ruptures

Imaging approaches strive for accurate representations of the sample ultrastructure, thus requiring minimal-invasive sample preparation procedures. Distortions and ruptures that can occur during the handling of the cells or tissue specimens and during expansion challenge the fidelity of any expansion-based SRM technology. Several strategies exist to assess the extent of distortions within ExM images[58]. Correlative comparisons between the diffraction-limited conventional images of the specimen before hydrogel embedding and ExSRRF images can help to identify ruptures and distortions on the microscale. However, to assess nanoscale ruptures and distortions, a super-resolved view of the pre-expansion ultrastructure has to be recorded using alternative super-resolution methods. Based on our experience from correlative comparisons of pre-hydrogel-embedded specimen and ExSRRF with both diffraction-limited microscopes and other SRM (that is, STED), gross artifacts that potentially interfere with biological information can often be sufficiently detected through comparisons with pre-hydrogel-embedded diffraction-limited microscopes, making pre- and post-expansion imaging using conventional microscopes a feasible, practical and valuable quality control step[40].

Although ruptures and distortions during the handling process may account for a large proportion of artifacts, other mechanisms may also cause alterations in the nano-architecture of the gel and tissue. Examples include inhomogeneities of the polymerized gel due to interactions with the sample structure or residual moisture during polymerization, mechanical heterogeneities of the sample and insufficient homogenization. To our knowledge, however, a thorough analysis of the degree to which each factor contributes is currently unavailable.

Selection of fluorescent dyes and proteins

When selecting fluorescent dyes or proteins for ExSRRF their suitability for both, the ExM and the eSRRF approach has to be evaluated. The classic 4× ExM protocols are generally compatible with many fluorescent dyes and fluorescent proteins. However, the degradation of fluorescent markers during the fixation, polymerization and homogenization process is an important consideration. For example, the signal quality of endogenous proteins such as GFP can be diminished under certain fixation conditions[59]. Additionally, while endogenous ß-barrel fluorescent proteins such as GFP display a high resistance to proteinase K digestion[60–62]

and are, therefore, likely to partially retain their endogenous fluorescence in the process of tissue processing[9], non-ß-barrel fluorescent proteins are more easily degraded by proteinase K digestion[62].

While, in principle, most ExM protocols are compatible with a large variety of fluorescent dyes, a reduction in fluorophore intensity after secondary antibody staining with a retention of 50% brightness compared with the pre-expansion signal is to be expected[9]. Furthermore, it is important to note that cyanine-family dyes such as Cy3, Cy5 and Alexa Fluor 647 show high degrees of degradation during hydrogel polymerization[9]. Atto 647N and CF 633 are commonly applied alternatives for the far-red channel as they exhibit good signal retention[9,40]. To achieve an additional resolution enhancement of ExM by fluctuation analysis, it is important to also take into account the emission properties of the fluorescent dyes or proteins. Without fluctuations in the fluorescence signal, eSRRF processing will not lead to an increase in resolution, whereas a high degree of fluorescence fluctuations enables high-quality super-resolved reconstructions. Supplementary Table 1 lists the dyes and fluorescent proteins and their expected performance in ExM and eSRRF.

Limitation to fixed samples

All expansion-based microscopy approaches are currently incompatible with live-cell imaging due to the requirement of fixation and homogenization and the separation of biomolecules[63].

Volumetric imaging

Two of the key advantages of standalone ExM are its ability to achieve isotropic expansion and resolution enhancement across all three dimensions, as well as the refractive index homogeneity of ExM-processed samples, both ideal traits for 3D super-resolution imaging of thick specimens. In contrast, eSRRF faces certain challenges for 3D super-resolution processing, particularly due to the requirements it places on the detection modality. Achieving resolution enhancement in all three dimensions necessitates simultaneous observation of fluorescence fluctuations across multiple *z*-planes. In practise, 3D-SRRF was demonstrated using a multifocus microscope, which employs a multifocus grating to project nine focal planes onto a single camera, enabling single-shot volumetric imaging[31]. However, this specialized detection system is not commercially available, limiting its accessibility to many researchers. Without such an instant volumetric imaging setup, eSRRF can only be applied to 3D datasets in a plane-by-plane fashion, improving resolution only in the lateral dimension. With this in mind, 3D ExSRRF can be implemented in a conventional microscope by acquiring sequences of up to 200 frames in each plane before moving on to the next *z*-position. Special caution has to be taken to avoid photobleaching during the *z*-stack acquisition.

Computational processing

eSRRF is an image processing technique relying on fluorescence fluctuations to reveal super-resolution information. If insufficient fluctuations are observable in the acquired data, for example, because of too long exposure times, eSRRF will not achieve a resolution enhancement. Also, the processing is highly nonlinear and can create artifacts, especially in cases of low signal-to-noise ratios. To identify and avoid artifacts, rigorous quality control based on quantitative image quality metrics is recommended. Finally, it has to be emphasized that due to the signal nonlinearity introduced by the processing, eSRRF reconstructions can not be used to compare signal levels quantitatively, but only to measure spatial signal patterns or distributions.

Experimental design

In the following sections of this protocol, we provide detailed information on how to successfully implement the method, including information and guidance on the materials, procedure, troubleshooting, and expected results. In this context, quality control is critical to ensure the results are interpretable and reliable. For example, it is important to conduct biological controls tailored to the experimental requirements, including the addition of biological positive and negative controls, as required. Furthermore, in the context of our method, specific technical controls should be implemented to avoid tissue-handling artifacts

that could interfere with biological interpretation. To address this, the protocol discusses various strategies for technical quality control, including thorough comparisons of pre- and post-expanded regions of interest and the use of computational quality control algorithms. For further details, refer to the respective sections below.

Expertise needed to implement the protocol

This protocol can be implemented by anyone with basic training in biological wet laboratory handling and fluorescence microscopy, therefore making it accessible to a broad range of users, including laboratory technicians, graduate students or postdoctoral researchers without requiring specialized facilities or additional personnel.

Regulatory approvals

No specific regulatory approvals, such as material transfer agreements or ethical permissions, are necessary for the basic implementation of this protocol in principle.

Materials

Biological materials and samples

- Tissue sections. We exemplify our protocol using ExSRRF images from FFPE kidney sections. The corresponding datasets and ethics approvals were published and described in the original publication[40]. As demonstrated, we anticipate that the protocol can, in principle, be used with any FFPE tissue type[40]
- Cells of interest. To demonstrate the SRRF/eSRRF principle, we used previously published live-cell HiLO-TIRF data of COS-7 cells (American Type Culture Collection cat. no. CRL-1651, RRID:CVCL_0224) expressing PrSS-mEmerald-KDEL marking the endoplasmic and DNA-PAINT microscopy data of immunolabeled microtubules in fixed COS-7 cells (datasets published by Laine and Heil et al.[31]). The cell lines used in your research should be regularly checked to ensure they are authentic and are not infected with mycoplasma
- Nanorulers. We exemplify photobleaching within our protocol using a time-stacked image series of 120 nm Nanorulers from GATTAquant DNA Nanotechnologies as previously described and published (datasets published by Kylies et al.[40])

Reagents

- Acryloyl-X, succinimidyl ester (Invitrogen, cat. no. A20770)
- Dimethyl sulfoxide (DMSO) (Invitrogen, cat. no. D12345)
  ▲ **CAUTION** DMSO is a combustible liquid and skin irritant. Avoid heat, hot surfaces, sparks, open flames and other ignition sources. Wear appropriate protective equipment and work under a fume hood. Dispose of contents to an approved waste disposal plant.
- 1× Dulbecco's phosphate-buffered saline (DPBS) (Gibco, cat. no. 14190094)
- Sodium acrylate (Sigma-Aldrich, cat. no. 408220)
  ▲ **CAUTION** Very toxic to aquatic life. Avoid release to the environment. Collect spillage and dispose of contents to an approved waste disposal plant. Wear appropriate protective equipment and work under a fume hood.
- Acrylamide (Sigma-Aldrich, cat. no. A3553)
  ▲ **CAUTION** Toxic if swallowed. Harmful in contact with eyes, skin or if inhaled. Reproductive toxicity, neurotoxic, and carcinogenic. Wear appropriate protective equipment and work under a fume hood. Dispose of contents to an approved waste disposal plant.
- *N*,*N*′-Methylenebis(acrylamide) (Sigma-Aldrich, cat. no. 146072)
  ▲ **CAUTION** Acute toxicity if swallowed. Harmful in contact with skin. Neurotoxicity, potential carcinogenicity, and reproductive toxicity. Wear appropriate protective equipment and work under a fume hood.
- ddH_2O

- Sodium chloride (NaCl; Sigma-Aldrich, cat. no. S7653)
- 4-Hydroxy-2,2,6,6-tetramethylpiperidine 1-oxyl (4HT) (Sigma-Aldrich, cat. no. 176141)
  ▲ **CAUTION** Harmful if swallowed. It causes serious eye damage and may cause damage to organs (liver, spleen) through prolonged or repeated exposure if swallowed. Wear appropriate protective equipment.
- *N*,*N*,*N*′,*N*′-Tetramethylethylenediamine (TEMED) (Sigma-Aldrich, cat. no. T9281)
  ▲ **CAUTION** Highly flammable liquid and vapor. Harmful if swallowed. Causes severe skin burns and eye damage. Toxic if inhaled. Wear appropriate protective equipment and work under a fume hood.
- Ammonium peroxodisulfate (APS) (PanReac AppliChem, cat. no. A1142,0250)
  ▲ **CAUTION** May intensify fire. Harmful if swallowed. Causes skin and serious eye irritation. May cause respiratory irritation after inhalation.
- Proteinase K from Tritirachium album (Sigma-Aldrich, cat. no. P2308)
- Tris-(hydroxymethyl)-amino methane (TRIS) (Carl Roth, cat. no. 5429.3)
- Ethylenediaminetetraacetic acid sodium salt (EDTA) (SERVA, cat. no. 11280.02)
  ▲ **CAUTION** Harmful if inhaled. May cause damage to organs through prolonged or repeated exposure. Wear appropriate protective equipment and work under a fume hood.
- Triton X-100 (Sigma-Aldrich, cat. no. T8787)
  ▲ **CAUTION** Toxic to aquatic life with long-lasting effects. Harmful if swallowed. Causes serious eye damage. Skin irritation. Avoid release to the environment. Collect spillage and dispose of contents to an approved waste disposal plant. Wear appropriate protective equipment and work under a fume hood.
- Poly-D-lysine solution, 1.0 mg/ml (Sigma-Aldrich, cat. no. A-003-E)
- ProLong Gold antifade mountant (Invitrogen, cat. no. P36930)
- Paraformaldehyde (PFA) (Sigma-Aldrich, cat. no. P6148)
  ▲ **CAUTION** Flammable solid. It is harmful if swallowed or inhaled. Causes serious eye damage. May cause cancer. Wear appropriate protective equipment and work under a fume hood.
- PFA, 32% wt/vol aq. soln., methanol free (Thermo Scientific Chemicals, cat. no. 047377.9L)
  ▲ **CAUTION** It is harmful if swallowed or inhaled. Causes skin corrosion and eye damage. May cause cancer. Wear appropriate protective equipment and work under a fume hood.
- Xylene, Baker Analyzed ACS (J.T. Baker, cat. no. 8080.2500)
  ▲ **CAUTION** Flammable liquid and vapor. May be fatal if swallowed and enters airways. Harmful if inhaled or in contact with skin. Wear appropriate protective equipment and work under a fume hood.
- Ethanol 99% denatured (Chemsolute, cat. no. 2212.5000)
  ▲ **CAUTION** Highly flammable liquid and vapor, causes serious eye irritation. Wear appropriate protective equipment and work under a fume hood.
- Dako target retrieval solution, pH 9, 10× (Agilent, cat. no. S236784-2)
- EnVision FLEX wash buffer, 20× (Agilent, cat. no. K800721-2)
- EnVision FLEX antibody diluent (Agilent, cat. no. K800621-2)

Equipment

General equipment and supplies

- Fume hood
- Laboratory gloves
- Safety glasses
- Respiratory protection (Filter type P1 or higher)
- SuperFrost Plus microscope slides (R. Langenbrinck, cat. no. 03-0060)
- Food steamer (any; we used Braun, model Multiquick FS 20)
- HybEZ oven (ACD, cat. no. 321720)
- HybEZ humidity control tray (ACD, cat. no. 310012)
- HybEZ humidifying paper (ACD, cat. no. 310025)
- EZ-Batch wash tray (ACD, cat. no. 321717)
- EZ-Batch slide holder (ACD, cat. no 321716)

- µ-Slide 2-well glass bottom (Ibidi, cat. no. 80287)
- 15 ml centrifuge tubes (Sarstedt, cat. no. 62.554.502)
- 50 ml centrifuge tubes (Sarstedt, cat. no. 62.547.254)
- 0.5 ml micro tubes (Sarstedt, cat. no. 72.699)
- 1.5 ml micro tubes (Sarstedt, cat. no. 72.690.001)
- 2 ml micro tubes (Sarstedt, cat. no. 72.695.500)
- Tissue culture dishes for adherent cells (Sarstedt, cat. no. 83.3903)
  ▲ **CRITICAL STEP** Using nonadherent culture dishes can lead to undesired effects during the gel mounting and humidifying step.
- Aluminum foil (any; we used Carl Roth, cat. no. 1770.1)
- Parafilm laboratory film (Amcor, cat. no. PM996)
- Cover glasses No.1, 24 ×24 mm (Marienfeld, cat. no. 0101060)
- Cover glasses No.1, 24 ×32 mm (Marienfeld, cat. no. 0101172)
- Cover glasses No.1, 24 ×46 mm (Marienfeld, cat. no. 0101202)
- Cover glasses No.1, 24 ×55 mm (Marienfeld, cat. no. 0101232)
- Forceps (any forceps are applicable; for example, Karl Hammacher, cat. no. HWC 071-10)
- Razor blades (any razor blade is applicable; for example, Lutz, cat. no. 43.10)
- Paint brushes (any paint brush is applicable; for example, Mucki, model Trigonomic, size 2 round, sizes 6 and 8 flat)
- Nail polish (any nail polish is applicable)
- pH meter (any pH meter is applicable; for example, Mettler Toledo, model SevenCompact S210)
- StainTray staining system with black lid (Simport Scientific, cat. no. M920-2)
- Pipette controller (any pipette controller is applicable; for example, Integra, model Pipetboy acu 2)
- 5 ml, 10 ml, 25 ml, 50 ml serological pipettes (Sarstedt, cat. nos. 86.1253.001, 86.1254.001, 86.1685.001, 86.1256.001)
- Pipette 0.1–2.5 µl (any pipette is applicable; for example, Eppendorf, model Research plus, cat. no. 3123000012)
- Pipette 0.5–10 µl (any pipette is applicable; for example, Eppendorf, model Research plus, cat. no. 3123000020)
- Pipettes 2–20 µl, 20–200 µl, 100–1,000 µl (any pipette is applicable; for example, Eppendorf, model Research plus 3-pack, cat. no. 3123000918)
- 10 µl, 200 µl, 1,000 µl pipette tips (Sarstedt, cat. nos. 70.3010.205, 70.3030.205, 70.3050.205)
- 3.5 ml transfer pipettes (any; we used Sarstedt, cat. no. 86.1171)
- Scissors (any scissors are applicable)
- Multipurpose paper cloths (any multipurpose paper cloths are applicable; for example, ZVG Multizell, cat. no. 10333-00)
- Delicate task wipes (any delicate task wipes are applicable; for example, Kimtech Science, cat. no 7558)
- Precision wipes (Kimtech Science, cat. no. 7552)
- ImmEdge hydrophobic barrier PAP pen (Vector Laboratories, cat. no. H-4000)
- 600 ml glass beaker (any 600 ml glass beaker is applicable; for example, DURAN, cat. no. 211064806)
- Magnetic stirrer (any magnetic stirrer is applicable; for example, Phoenix, model RSM-10 HS)
- Staining jars Hellendhal (Kartell, cat. no. 355)
- Staining troughs with lids (Carl Roth, cat. no. H554.1)
- Glass inserts for staining trough (Carl Roth, cat. no. H552.1)
- Wire hangers for glass staining rack (Carl Roth, cat. no. H553.1)
- Analytical balance (Sartorius, model no. Entris II BCE224I-1S)
- Precision balance (Sartorius, model no. Quintix 5102-1S)

Fluorescence microscope

The images presented here were captured using a THUNDER Imager 3D Live Cell and 3D Cell Culture (Leica Microsystems) equipped with a 20× objective (NA, 0.40) for low-magnification and a 40× objective (NA, 1.10), 63× objective (NA, 1.10) and 100× objective (NA, 1.47) for high-magnification imaging.

Data processing and analysis tools/software

- Analysis computer: a computer with a Microsoft Windows 64-bit or MacOS operating system and Java 8. See 'Equipment setup' for hardware requirements
- Analysis software: See 'Equipment setup' for software setup details

Reagent setup

4% (wt/vol) PFA

For a 4% (wt/vol) PFA solution, dissolve PFA powder in 1× PBS to achieve a concentration of 4% (wt/vol). Aid solubilization by stirring, heating to 50–60 °C, and adding up to ten drops of 1 M NaOH per 500 ml. Aliquoted 4% PFA solution can be stored at −20 °C for at least 6 months. Instead of using PFA powder to create the final 4% (wt/vol) PFA solution, alternatively a commercially available 32% (wt/vol) PFA stock solution can be purchased, stored safely at room temperature (20–25 °C) and diluted with 1× PBS to achieve the final 4% (wt/vol) PFA solution used for sample fixation.

▲ **CRITICAL STEP** Avoid long-term storage of 4% PFA solution at 4 °C or room temperature as it results in PFA degradation and the generation of formic acid, which is toxic and diminishes the efficiency of PFA fixation.

Acryloyl-X stock solution (10.0 mg/ml)

Dissolve Acryloyl-X powder in anhydrous DMSO at a concentration of 10.0 mg/ml at room temperature, aid solubilization by using a bench-top shaker. Aliquot dissolved Acryloyl-X in portions of 15µl at −20 °C for long-term storage. Acryloyl-X can be stored for at least 6–9 months. While in general, repeated freeze–thaw cycles of Acryloyl-X solutions should be avoided, we encountered no problems reusing Acryloyl-X stock solutions after 1–3 freeze–thaw cycles.

Acryloyl-X anchoring solution (0.1 mg/ml)

Thaw Acryloyl-X stock solution aliquot (10.0 mg/ml) and dilute in PBS to achieve a final concentration of 0.1 mg/ml. For the anchoring treatment of a clinical histology section, depending on sample size, ~100–200 µl of anchoring solution is required.

Proteinase K aliquot

Dissolve lyophilized proteinase K powder (≥30 units/mg) in ddH_2O at room temperature to achieve a concentration of 10 mg/ml (300 U/ml), then distribute to aliquots of appropriate volume (for example, 150 µl). Proteinase K aliquots can be stored at −20 °C for at least 6 months.

▲ **CRITICAL STEP** Avoid freeze–thaw cycles as they may damage Proteinase K, resulting in reduced enzymatic activity and suboptimal experimental results.

Digestion buffer

The digestion buffer consists of 50 mM Tris, 25 mM EDTA, 0.5% Triton X-100 and 0.8 M NaCl. Titrate the digestion buffer to pH 8. When using 50 mM Tris base to create the digestion buffer as described above, the solution generally is expected to be too basic, requiring acidification (that is, using hydrochloric acid). Alternatively, a Tris–HCl solution at pH 8 can be used instead of Tris base, which generally does not require further pH adjustments, as described elsewhere[62]. The digestion buffer can be stored as aliquots at −20 °C for at least 6 months.

Digestion solution

Acclimate digestion buffer and proteinase K to room temperature, then add proteinase K at a concentration of 4–12 U/ml. For most pathology samples, a concentration of 8 U/ml is appropriate. Mix using a 1,000 µl pipette tip or a 5 ml serological pipette.

▲ **CRITICAL STEP** Avoid using benchtop shakers as their use may damage proteinase K, resulting in reduced enzymatic activity and suboptimal experimental results. Carefully pipette to mix the solution instead.
▲ **CRITICAL STEP** Always prepare a fresh digestion solution before starting the digestion step. Proteinase K activity could diminish over time at 4 °C or room temperature, resulting in reduced enzymatic activity and suboptimal experimental results.

Target retrieval solution
Dilute DAKO target retrieval pH 9 stock solution (10×) in ddH_2O to achieve a 1×solution. Mix up and down using a 50 ml serological pipette until solution is fully mixed.

Agilent wash buffer solution
Dilute EnVision FLEX wash buffer stock solution (20×) in ddH_2O to achieve a 1× solution. Mix up and down using a 50 ml serological pipette until solution is fully mixed. Make sure not to introduce bubbles.

Monomer solution
The monomer solution consists of 1× PBS, 2 M NaCl, 8.625% sodium acrylate, 2.5% acrylamide and 0.1% *N*-*N*′-methylenbis-(acrylamide). The monomer solution can be aliquoted and stored at −20 °C for 1–6 months.
▲ **CRITICAL STEP** The quality of sodium acrylate may vary. Low-purity sodium acrylate dissolved in water can appear slightly yellow. In this case, it is recommended to switch to a new batch.
▲ **CRITICAL STEP** For long-term storage, the monomer solution should be stored at −20 °C as prolonged storage at 4 °C may result in accelerated decay and suboptimal results. For immediate use, monomer solution should always be handled at 4 °C to avoid premature polymerization. We have successfully used batches of monomer solution that were stored at 4 °C for several months. However, after prolonged storage (that is, >3–6 months) at 4 °C, we noted precipitation within the monomer solution and encountered suboptimal results and tissue artifacts. We, therefore, recommend not storing the monomer solution at 4 °C for prolonged times but rather thawing fresh aliquots.

4HT stock solution
To generate 10 ml of 4HT stock solution, mix 50 mg of 4HT with an appropriate amount of ddH_2O until a total volume of 10 ml is reached. The solution can be aliquoted into appropriate portions (that is, 1 ml) and stored at −20 °C for at least 4 weeks. Although a short storage period is recommended, we found that significantly longer storage times (that is, up to 3–6 months at 4 °C) can still yield satisfactory results.

APS stock solution
To generate 10 ml of APS stock solution, mix 1 g of APS with an appropriate amount of ddH_2O until a total volume of 10 ml is reached. The solution can be aliquoted into smaller portions (that is, 1 ml) and stored at −20 °C for at least 2 weeks. Although a short storage time is recommended, we found that significantly longer storage times (that is, up to 3–6 months at 4 °C) can still yield satisfactory results.

TEMED stock solution
To generate 10 ml of TEMED stock solution, mix 1 ml of TEMED with an appropriate amount of ddH_2O until a total volume of 10 ml is reached. The solution can be aliquoted into appropriate portions (that is, 1 ml) and stored at −20 °C for at least 2 weeks. Although a short storage time is recommended, we found that significantly longer storage times (that is, up to 3–6 months at 4 °C) can still yield satisfactory results.

Activated gelling solution
The appropriate amount per clinical histology sample is in the range of 200 µl. To generate 200 µl of the activated gelling solution, mix monomer solution with 4HT, TEMED and APS

stock solutions in this order on ice in a ratio of 188:4:4:4 (188 ml of monomer solution, 4 ml of 4HT, 4 ml of TEMED and 4 ml of APS) to achieve final concentrations of 0.01% 4HT, 0.2% TEMED and 0.2% APS in a 1.5 or 2.0 ml Eppendorf safe-lock tube. Briefly vortex the solution to mix the individual components.

▲ **CRITICAL STEP** The activated gelling solution must be freshly prepared on ice immediately before sample incubation. Adding APS as the last component is important as it initiates the gel polymerization. In addition, as polymerization is a temperature-dependent reaction, it is critical to work on ice to avoid premature gelation.

▲ **CRITICAL STEP** The concentration of the inhibitor solution 4HT can be adjusted depending on the experimental design, such as the thickness of the biological sample. Thinner sections or cultured cells can be penetrated more efficiently by the activated gelling solution. Therefore, lower concentrations of 4HT can be utilized in these cases.

Equipment setup

Analysis computer

We recommend performing the image processing and analysis steps on a separate analysis workstation (Windows PC or Mac with Java 8) with OpenCL-compatible GPU resources. The analysis in this protocol was performed with a MacBook Pro with an Intel Core i9 CPU, 2.3 GHz, 8 cores, AMD Radeon Pro 5500M GPU and 32 GB RAM and a Windows workstation with an Intel Core i9 CPU, 3.0 GHz, 24 cores, RTX NVIDIA 4090 with 24 GB and 128 GB RAM.

Analysis software

Image processing can be performed using ImageJ/Fiji or Python. Both implementations are optimized for GPU processing, and while the NanoJ implementations in ImageJ/Fiji might be more user-friendly for an easy start[64,65], the Nanopyx Python library and notebooks offer a pathway to automation and integration into Python-based image processing workflows for more experienced users[66].

To set up image processing tools with ImageJ/Fiji, download the application (https://imagej.net/software/fiji/), and unpack it in a location that is not 'C:\Program Files' but, for example, 'C:\Users\[your name]\'. Run the application and update via 'Help > Update ....'. If you are running ImageJ/Fiji for the first time, you will have to restart the application and run 'Help > Update ....' a second time to add update sites (detailed instructions on https://github.com/HenriquesLab/NanoJ-eSRRF). Add the update sites NanoJ-Core and NanoJ-Squirrel from the list of sites and manually add the NanoJ-eSRRF update site with the link 'https://sites.imagej.net/NanoJ-LiveSRRF/' at the end of the list. After running the update and restarting ImageJ/Fiji, all plugins should be available in the 'Plugins' menu.

For Python-based image processing tools available in the NanoPyx library, you will find documentation and tutorials here: https://github.com/HenriquesLab/NanoPyx. All the tools used in this protocol are available as NanoPyx Jupyter notebooks (https://github.com/HenriquesLab/NanoPyx/blob/main/notebooks).

▲ **CRITICAL STEP** If you have issues installing or running the applications, check the issues on the respective GitHub site or post your own questions. You will find a very helpful and engaged bioimage analysis community that is always within reach at https://forum.image.sc/.

Procedure

Molecular labeling of specimen

● **TIMING overnight Bench time: 4 h**

Depending on the experimental setup, different labeling approaches may be applicable. In this protocol, we focus on describing one robust immunofluorescence-based labeling approach for FFPE human clinical and experimental animal specimens.

1. Dewaxing and rehydration of samples
   Sequentially immerse sections in xylene, ethanol and ddH_2O for dewaxing and rehydration.

2. Target retrieval
   To perform heat-based antigen retrieval, incubate the specimen in an appropriate heated target retrieval solution. Allow the sample to cool down for an appropriate amount of time.
3. Hydrophobic barrier
   Draw a hydrophobic barrier around the specimen using an appropriate hydrophobic barrier pen to contain the reagents in place during the subsequent steps.
4. Primary antibody staining
   Mix primary antibodies and appropriate buffer in the desired ratio. Then, incubate in a humidified container.
5. Secondary antibody staining
   After primary antibody labeling, remove the primary antibody solution followed by subsequent washing steps to remove unbound primary antibody. Next, incubate the sections with appropriate secondary antibodies and a nuclear marker in an appropriate buffer. Incubate the samples in a humidified container shielded from light. After incubation remove unbound antibodies by washing the sample.
6. Mounting
   Add one drop of mounting solution and carefully place an appropriate coverslip on top of the section without introducing bubbles between the coverslip and the sample. (Optional stop) Stained and mounted sections can be stored at room temperature for up to 2–4 weeks. Protect the samples from light to avoid bleaching.

Pre-expansion imaging

● **TIMING 1–2 h**

Pre-expansion imaging is an important aspect of the ExSRRF workflow to ensure accurate and reliable results and quality control.

7. Pre-expansion imaging
   Mount the specimen on the microscope, set up the required channels and scan the whole tissue specimen at the desired optical magnification. For large samples, it is advised to use a low-magnification objective (for example, 10× or 20×) for the overview scan of the whole sample, followed by high-resolution imaging of regions of interest (for example, 40× or 63× magnification). Use the stitching function to create an overview of the whole tissue section.
   ▲ **CRITICAL STEP** When performing conventional pre-expansion imaging, the optical setup should match or come close to the desired imaging settings to allow optimal comparison and assessment of the expansion factor.
   ▲ **CRITICAL STEP** We recommend scanning the entire tissue specimen during pre-expansion imaging as this ensures that the ROI for ExSRRF imaging is captured, allowing for correlative conventional and post-ExSRRF comparisons. Whole specimen imaging also helps to navigate the specimen and allows to crop larger pieces of tissue before hydrogel embedding if necessary.
   (Optional stop) Stained and mounted sections can be stored at room temperature for up to 2–4 weeks. Protect the samples from light to avoid bleaching.
   ◆ **TROUBLESHOOTING**

Anchoring

● **TIMING overnight Bench time: 15 min**

8. Coverslip removal
   Remove the coverslip by first immersing the sample in xylene, ethanol and ddH_2O to remove the nail polish and to soften the mounting media, then carefully insert a razor blade between the slide and the coverslip and lift the coverslip (Extended Data Fig. 1).
   ◆ **TROUBLESHOOTING**
9. Anchoring treatment
   Mix the acryloyl-X anchoring solution as described in the 'Reagents setup' section and pipette an appropriate amount onto the section. Then, incubate the section at room temperature overnight in a humidified container shielded from light.

Polymerization

● **TIMING 3 h Bench time: 30 min**

▲ **CRITICAL** During the polymerization step, the stained tissue sections are transformed into a tissue–hydrogel hybrid, ultimately allowing for subsequent tissue expansion. One of the key considerations is that the polymerization is a temperature-sensitive reaction: While some steps must strictly be carried out at 4 °C to avoid premature gelation, others require incubation at 37 °C to facilitate gel polymerization.

10. Washing off the anchoring solution
    Remove the acryloyl-X solution from the tissue section and wash off the remaining acryloyl-X solution using 1× PBS.
11. Preparation of activated gelling solution
    Prepare activated gelling solution on ice as described in the 'Reagent setup' section of the protocol.
12. Gelling solution penetration step
    Pipette an appropriate amount of activated gelling solution on the tissue section, immediately move samples to 4 °C and incubate them in a humidified container protected from light for 30 min (Extended Data Fig. 2a).
    ◆ **TROUBLESHOOTING**
13. Assembly of gelling chamber
    Construct the gelling chamber by placing two coverslips as spacers on each side of the tissue section, then lay a third, large coverslip on top of the two spacers.
    ◆ **TROUBLESHOOTING**
14. Hydrogel polymerization step
    Incubate the specimen for at least 2 h at 37 °C in a pre-heated incubator protected from light. After completion of the polymerization step, cool down the samples to 4 °C.
    ◆ **TROUBLESHOOTING**
    (Optional stop) After gelation, sections can be stored in a humidified container, protected from light with intact gelling chamber for up to 1 week at 4 °C.

Digestion

● **TIMING 4.5 h Bench time: 30 min**

During the digestion step the sample is homogenized to enable isotropic expansion in the subsequent steps.

15. Preparation of digestion solution
    Prepare the digestion solution at room temperature as described in the reagent setup by mixing the digestion buffer and an appropriate amount of the proteinase K aliquot.
16. Disassembly of the gelling chamber and gel trimming
    To disassemble the gelling chamber, first carefully lift the top coverslip with the help of a razor blade that is inserted into the space between the top and the spacer coverslips. Next, remove the spacer coverslips following a similar procedure. After disassembly of the gelling chamber trim the sample by removing excess gel laterally of the tissue section (Extended Data Fig. 3a,b).
    ◆ **TROUBLESHOOTING**
17. Incubation
    Incubate the sample in digestion solution in a humidified incubator at 60 °C for 4.0–4.5 h. Ensure that the digestion solution does not evaporate during the incubation step, that is, by placing a piece of Parafilm on top of the tissue section immersed in digestion solution. Refer to Extended Data Fig. 3c,d and Supplementary Note 2, step 17 for a detailed description of this step.
18. Cool down
    After incubation, move the tray to 4 °C to allow the sections to cool down. (Optional stop) Following digestion, tissue–gel hybrids can be stored in a humidified container with a Parafilm cover on top in the dark at 4 °C for several days. As long as the Parafilm fully covers the section, no additional buffer or storing solution is required as the Parafilm prevents dehydration.

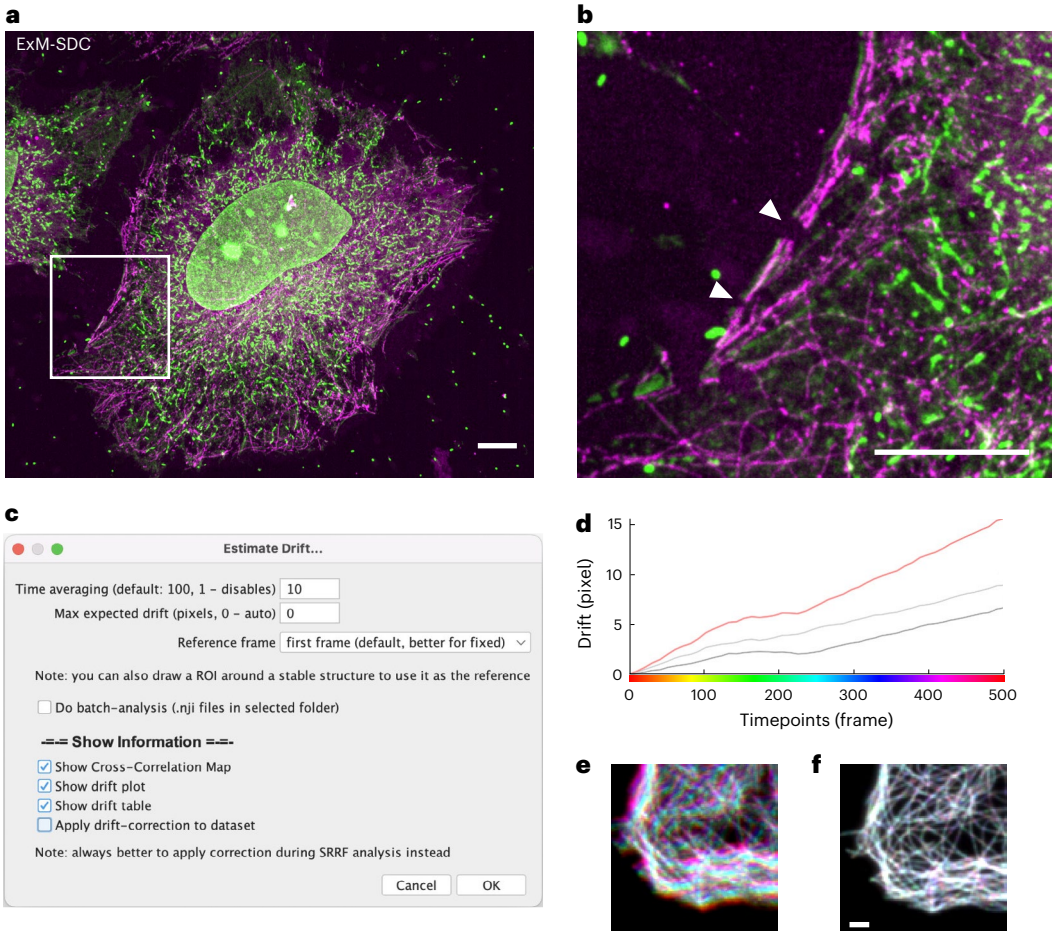

Fig. 2 | Recognizing and troubleshooting ExSRRF-related artifacts. a,**b**, In Step 23 it is critical to identify expansion-related ruptures of subcellular structures: here, we see CHO cells in 4× ExM with post-expansion pan- and immune labeling (Bodypi-NHS (green), with anti-beta tubulin + Fab Alexa 647 (magenta)), acquired with a spinning disc confocal (SDC) microscope (**a**), and the zoom-in shows discontinuities of the microtubule network (white arrowheads) due to insufficient homogenization, leading to ruptures in the structure during the expansion process (**b**). To avoid resolution loss due to motion artifacts, the sample drift should be either corrected with NanoJ-Core in Step 25 or directly in the eSRRF processing in Step 29. **c**, Settings for NanoJ-Core drift estimation. **d**, Based on cross-correlation, the drift in the *x* direction (black line) and *y* direction (gray line) and total drift displacement (red line) against the first frame is calculated for each frame of the example dataset (WF dataset of immunolabeled microtubules in fixed COS-7 cells published by Laine et al.[31]). **e**,**f**, The sample drift observed in **e**, the example dataset, highlighted here by a temporal color projection (color scale in **d**), can be successfully corrected (**d**), leading to a nice overlap of the image features throughout the whole time series (**f**). Scale bars, 20 µm (**a**,**b**); 2 µm (**f**).

Tissue expansion

● **TIMING 1.5 h Bench time: 30 min**

The tissue expansion stage of this manuscript requires careful handling to prevent overall sample damage and distortions.

19. Removal of the tissue section and placement in the expansion chamber
Carefully separate the tissue–hydrogel hybrid specimen from the slide by carefully inserting a wetted razor blade at a sharp angle between the slide and the specimen. Use a soft and wet paintbrush to load the tissue onto the razor blade after detaching from the slide. Transfer the tissue using the razor blade to a wetted cell culture well with the help of the paintbrush.

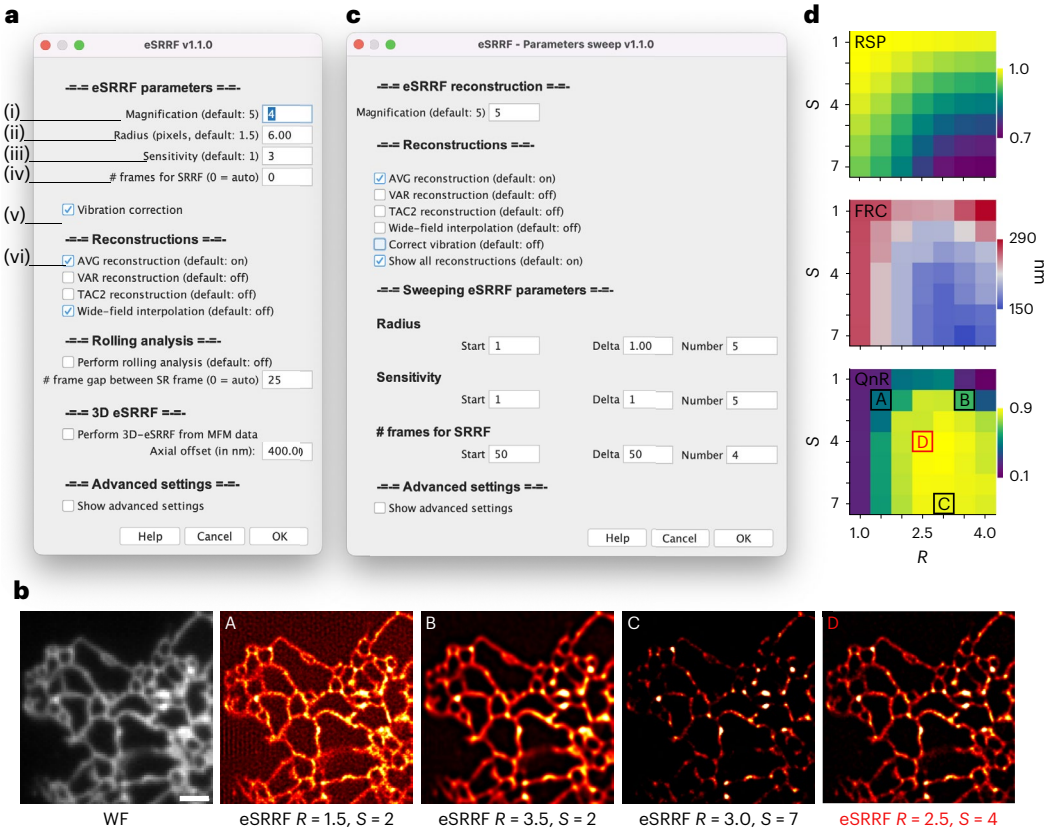

Fig. 3 | eSRRF processing and parameter sweep. a, NanoJ-eSRRF includes the following main processing parameters: (i) magnification *M*; (ii) ring radius *R*; (iii) sensitivity *S*; (iv) frames per timepoint; (v) vibration correction; and (vi) the temporal reconstruction mode (AVG, VAR or TAC2). **b**, WF and eSRRF reconstructions for various parameter combinations of live-cell HiLO-TIRF data of COS-7 cells expressing PrSS-mEmerald KDEL marking the endoplasmic reticulum (dataset published by Laine and Heil et al.[31]). **c**, To find the optimal parameter combination, a parameter range based on a Start value, an interval Delta and the number of steps is defined in the eSRRF–parameter sweep. **d**, The sweep outputs are RSP-based fidelity (top) and an FRC-based resolution map (middle), which are translated into a QnR map (bottom), representing the compromise of both image quality metrics. This way, the parameter sweep allows for quantitative assessment of reconstruction quality and resolution, reporting low QnR scores for patterning artifacts (**b**, example A), low-resolution reconstructions (**b**, example B) or over-sharpening artifacts (**b**, example C), and QnR maxima for the optimal eSRRF reconstruction parameters (**b**, example D). The imaging data used for the visualizations and analysis displayed in this figure were acquired using a WF fluorescence microscope with highly inclined laser illumination (HiLO). Scale bar, 2 µm (**b**).

20. Tissue expansion

    Incubate the tissue–hydrogel hybrid in ddH_2O by carefully applying ddH_2O to the tissue section using an excess amount of ddH_2O in relation to the size of the specimen. Then, incubate the specimen protected from light in ddH_2O at room temperature for 15 min. Carefully remove the ddH_2O and repeat the procedure of incubating the specimen in fresh ddH_2O three more times until a total incubation time of 60 min is reached (Extended Data Fig. 4a,b).

    (Optional stop) The specimen can be stored at 4 °C protected from light for at least 1–2 weeks in its expanded state in a humidified container. Despite the storage in a humidified container, we advise rehydrating the expanded specimen with a few drops of deionized water every other day to prevent dehydration and the introduction of dehydration-based artifacts (for example, the introduction of gel ruptures from inhomogeneous dehydration while attached to a poly-lysine-coated coverslip). Alternatively, for long-term storage, the expanded specimen can be transferred to PBS at 4 °C. Transfer of the expanded specimen to PBS causes

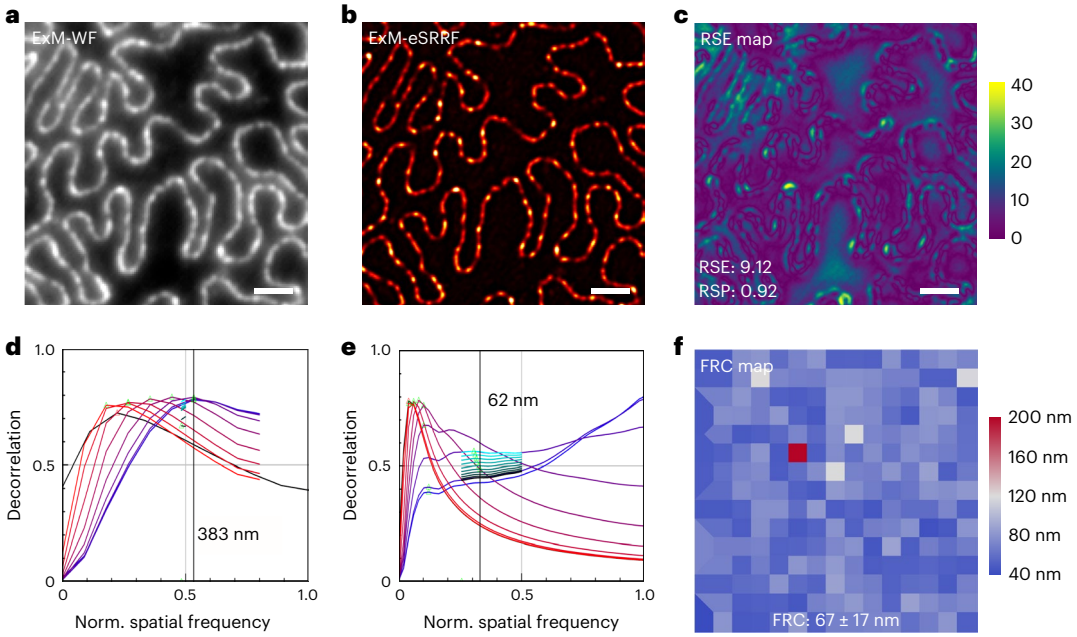

Fig. 4 | Assessing reconstruction performance with quantitative image quality metrics. a–**c**, Processing artifacts can be localized based on a quantitative comparison of the WF (**a**) and super-resolved image (**b**) based on mapping the resolution scaled error (RSE) (**c**). The map highlights areas of low fidelity in yellow. The global error metric RSP is normalized (norm.) to a range of 1 and allows to compare performance between imaging regions. **d**,**e**, Resolution enhancement is estimated based on decorrelation analysis of the WF (383 nm) (**d**) and eSRRF (62 nm) reconstruction (**e**). **f**, Local variations in image resolution can be mapped by FRC analysis. The imaging data used for the visualizations and analysis displayed in this figure were acquired with a WF fluorescence microscope. Scale bars, 2 µm (**a**–**c**).

the gel to shrink, which is to be expected and does not cause a damage to the specimen. After recovery from PBS, the sample can be expanded again safely using deionized water.

◆ **TROUBLESHOOTING**

Sample mounting

● **TIMING 15 min Bench time: 15 min**

We here discuss a poly-D-lysine-based strategy for sample mounting and immobilization in glass-bottom chamber slides (such as the Ibidi µ-Slide 2-well glass-bottom imaging chambers). However, depending on experimental requirements, local setups and expertise, other mounting strategies may also be applicable and have successfully been used for mounting and immobilizing expanded specimen as well. Examples of alternative sample mounting strategies include poly-L-lysine, agarose and superglue[62] with or without additional physical immobilization strategies such as two-component silicone glue[24]. For additional mounting strategies refer to Supplementary Note 1.

21. Coating of imaging chambers
    Coat the Ibidi µ-Slide 2-well glass-bottom imaging chambers by fully covering the entire bottom surface with an appropriate amount (that is, 1 ml) of poly-D-lysine for 20 min at room temperature. After completing the incubation, remove poly-D-lysine and dry slides at room temperature or on a heat plate at 37 °C until the surface is dry.
22. Sample mounting in glass-bottom chamber
    Trim a piece of aluminum foil to a width slightly smaller than the width of the imaging chamber slide that will be used for imaging. Next, transfer the expanded specimen from the cell culture well onto the trimmed piece of aluminum foil with the help of a soft paintbrush. Use the aluminum foil to transfer the specimen to the coated imaging chamber and use a

soft paint brush to gently push the specimen off the aluminum foil and into the imaging chamber. Carefully remove excess liquid using a thin piece of laboratory paper (Extended Data Fig. 4c,d).
(Optional stop) Samples mounted in imaging chambers can be stored at 4 °C, protected from light, for several days. However, to avoid dehydration, the samples should be rehydrated with a few drops of ddH_2O every day. Avoid excess fluid, as this could interfere with the poly-D-lysine coating, causing lateral movement during image acquisition.

Post-expansion imaging

● **TIMING 2 h**

23. Identifying the *z*-plane and creating a tissue overview
Transfer the specimen mounted in the imaging chamber to the microscope and place the imaging chamber in the slide holder of the microscope. Select a non-immersion objective with a large working distance (that is, a 10× or 20× objective). Grossly adjust the *xy*-position within the microscope so that the objective aligns with the middle of the specimen. Set the *z*-position to a level that is distant from the expected focus plane of the tissue section. Set the appropriate imaging channels within the microscopy settings. Activate the fluorescence detection and slowly move the *z*-position toward the sample until the signal appears. After adjusting the *z*-position, we recommend creating a tissue overview using a 10× or 20× objective, either using all channels or a single channel, to visualize identifiable tissue landmarks for general orientation.
▲ **CRITICAL STEP** We recommend starting to image in the middle of the sample as the gel margin does not contain tissue. Initially, we recommend imaging a strongly and ubiquitously expressed marker while using sufficient laser or LED power as the signal intensity in expanded samples may be lower than expected.
▲ **CRITICAL STEP** During the acquisition, the data should be visually inspected to identify gross artifacts such as tears, distortions or incomplete structures (Fig. 2a,b and Supplementary Fig. 1). This can be achieved by aligning pre- and post-expansion tissue overviews. Note that the pre-expansion overview may need to be flipped and rotated to match the post-expansion overview (that is, using the imaging software of the microscope or third party image analysis software such as ImageJ or FIJI).
◆ **TROUBLESHOOTING**
24. Setting-up image settings and timelapse image acquisition
Change the objective to the higher magnification immersion objective with good NA for timelapse image acquisition. First, re-adjust the *z*-position in case of a *z*-position offset from changing objectives. Next, optimize image acquisition parameters for all channels to yield optimal image quality when obtaining single images in each channel. After adjusting the imaging parameters, select the ROI and acquire a single reference image that can be matched to the pre-expansion image to assess expansion factor and sample distortions. Then, select timelapse acquisition within the system software. Set the desired number of frames within the ROI and minimize the time in between the acquisition of the individual frames to 20–50 Hz. A good initial starting point is either capturing 200 frames or adjusting the imaging parameters to acquire a time stack within 30–90 s. Then, proceed with acquiring the timelapse image series of the ROI.
▲ **CRITICAL STEP** When adjusting image acquisition parameters, in some cases, a slight compromise between optimal signal quality and exposure time is necessary as the eSRRF algorithm needs the detection of fluorescent fluctuations over time at acquisition rates of 20–50 Hz, whose detection can be impaired with low frame rates under 10 Hz. While the illumination power should provide high signal levels, signal bleaching and saturation should be avoided. Severe signal loss due to bleaching or *z*-drift cannot be corrected; these datasets may need to be discarded. Refer to Step 28 for further information on eSRRF parameter optimization.
▲ **CRITICAL STEP** For multichannel imaging, proceed as follows: always acquire the full time series of one channel before moving to the next, starting with the longest wavelength and proceeding to shorter wavelengths (for example, red, orange and green). Some channels,

such as nuclear staining, may not be relevant for super-resolution processing. In such cases, a good strategy is to capture a single reference image first, then deactivate unnecessary channels for timelapse acquisition to optimize both time efficiency and storage capacity.
◆ **TROUBLESHOOTING**

Pre-processing quality control and correction

● **TIMING 2 h**

25. Correcting movement artifacts
The presence of lateral movements in timelapse image series will generate drift artifacts during eSRRF processing. If lateral movement artifacts are observed, an image registration for drift correction should be applied. This can be done, for example, with NanoPyx Jupyter notebooks (https://github.com/HenriquesLab/NanoPyx/blob/main/notebooks/DriftCorrection.ipynb)[66] or with the ImageJ/Fiji plugin NanoJ-Core (Plugins > NanoJ-Core > Drift Correction > Estimate Drift). The drift correction is performed based on image cross-correlation (Fig. 2c–f). To speed up the calculation, a frame window for 'Time averaging' is defined. It should be large enough to result in a continuous progression of the drift while also picking up on vibrations on smaller timescales. To avoid overestimation of the drift, a maximum value ('Max expected drift') can be defined while the 'Reference frame' should be the first frame in the stack. The resulting drift values will be saved in a drift table. To achieve optimal results, the drift correction should be directly applied during eSRRF processing (Step 28). A test dataset for drift correction can be found here: https://doi.org/10.5281/zenodo.11518140 (ref. 67).
26. Channel registration for multicolor data
In the case of multichannel data an additional channel registration might be required, which can also be performed with NanoPyx (https://github.com/HenriquesLab/NanoPyx/blob/main/notebooks/ChannelRegistration.ipynb) or the ImageJ/Fiji plugin NanoJ-Core (Plugins > NanoJ-Core > Registration > Register Channels - Estimate). For channel registration, a 'Reference channel' has to be chosen onto which other channels are mapped and the 'Number of channels in the dataset' must be specified. To avoid overestimation, a maximum shift value can be defined, as well as the block size ('Blocks per axis'), the lower limit of the similarity ('Min similarity') and the degree of blurring ('Gaussian blur radius'). To get started, the use of default values is recommended. Registration results will be saved in a results table and can be directly applied by activating the 'Apply channel-realignment to dataset' option or running Plugins > NanoJ-Core > Registration > Register Channels - Apply.

Computational image enhancement

● **TIMING 1–2 h**

27. Set up eSRRF
eSRRF is available as ImageJ/Fiji plugin (see the 'Software setup' section) and as NanoPyx Jupyter notebooks (https://github.com/HenriquesLab/NanoPyx/blob/main/notebooks/eSRRFandQC.ipynb).
While we recommend eSRRF for super-resolution processing, we still provide alternative instructions for steps 27–29 for SRRF processing in Supplementary Note 3.
28. Optimizing the image-processing parameters
There are five eSRRF processing parameters (Fig. 3a) that should be chosen with the following rationale:
    - The magnification parameter should be set based on an estimate of the smallest feature size expected to be observed in the sample architecture while taking into account the expansion factor. Following the Nyquist criterion, this should result in an effective pixel size (raw image pixel size divided by the expansion factor) of half the feature size. Considering the resolution power of eSRRF and computation time the effective pixel size should not be much smaller than 10 nm. The default parameter is a magnification of 5, resulting in 8 nm pixels in the eSRRF reconstruction of the ExM raw data with a pixel size of 160 nm and an expansion factor of 4

- The ring radius has the most pronounced impact on the results, and it is directly related to the width of the underlying point spread function. Choosing a too-small ring radius will create patterning artifacts (Fig. 3b, example A), while too-large values result in signal blurring and low-resolution outcomes (Fig. 3b, example B). The default parameter is 0.5 pixels
- The sensitivity allows you to fine-tune the PSF sharpening power applied. The default value is 1, and the optimal setting should be determined in a parameter sweep against the ring radius, as described below. Too high values create over-sharpening artifacts (Fig. 3b, example C)
- The frames per timepoint define the size of the window for the temporal analysis. To avoid movement artifacts, the time window should be as short as possible while providing enough temporal information for eSRRF reconstruction. A good practice is to test reconstruction quality with 50 frames, 100 frames, 150 frames and 200 frames. The reconstruction quality will saturate at large temporal window sizes and the shortest window close to the maximum quality score should be chosen
- Vibrations or sample drift can be compensated during eSRRF processing by activating the 'vibration correction' option (Supplementary Fig. 2)
- In eSRRF, different temporal analysis strategies can be activated as eSRRF reconstructions. The default is the 'AVG', a reconstruction based on temporal averaging. This will yield in the best reconstruction results for most datasets. In the case of datasets that display sparser blinking patterns, more similar to a single molecule localization microscopy dataset, higher order reconstructions such as 'VAR' or 'TAC2' can yield better results. However, these reconstruction modes are also more prone to create artifacts and have to be used with rigorous quality control[31]

While magnification and frames per timepoint can be estimated based on the experimental conditions, other parameters should be optimized based on a parameter sweep. For this purpose, eSRRF has an automated function that allows to directly quantify resolution and fidelity of the different reconstructions and compare the performance based on the quality and resolution (QnR) score (Fig. 3c,d). The parameter sweep is performed with NanoJ-eSRRF (Plugins > NanoJ-eSRRF> eSRRF – Parameter Sweep) (Fig. 3c). To reduce processing time, perform the optimization procedure on a representative crop region of the raw data image stack (for example, 100 × 100 pixels). The sweep output will be an image stack of all reconstructions and sweep maps of the resolution (Fourier ring correlation (FRC) map) and fidelity values (resolution-scaled Pearson (RSP) map). The best compromise between resolution can be identified as a maximum in the QnR map that is calculated based on the sweep outputs (Plugins > NanoJ-eSRRF> eSRRF – Get QnR map from sweep output; Fig. 3d). The eSRRF reconstruction with the optimal processing parameters identified in this way yield in a high-quality reconstruction providing good image resolution and image fidelity at the same time (Fig. 3b, example D).

▲ **CRITICAL STEP** To identify optimal reconstruction parameter settings with the parameter sweep, it has to be performed in the right parameter range. An indicator that the range is not optimal is if QnR maximum is located at the edge of the sweep map. If this is the case, adjust the range and rerun the sweep. It is also important to visually inspect and compare the reconstructions as a control. This will be much easier if the contrast of the stack of eSRRF reconstructions is normalized (Plugins > NanoJ-eSRRF> eSRRF Tools > Reset stack for display…). For training purposes, we are providing a training manual with test datasets and parameter recommendations here: https://zenodo.org/doi/10.5281/zenodo.11518140 (ref. 67).

29. eSRRF processing

Based on the optimal parameter set identified in the parameter sweep (Step 28) the full raw dataset is processed. For each dataset you will get a WF and a super-resolved eSRRF reconstruction. As mentioned above all of this can also been done with the NanoPyx implementation, detailed instructions are found in the training manual (https://doi.org/10.5281/zenodo.11518140)[67]. Consider batch processing to automate the image

reconstruction, for example, via ImageJ macro scripts (https://github.com/HenriquesLab/NanoJ-eSRRF/wiki/Batch-processing).

▲ **CRITICAL STEP** To accurately measure absolute distances and perform quantitative image analysis, it is essential to define the correct pixel size based on the effective magnification in the final image reconstruction (Image > Properties). This involves calculating the correct pixel size by dividing the original pixel size by the measured expansion factor. Adjusting the pixel size in this manner ensures that any measurements or analyses reflect the true, scaled dimensions of the sample post-expansion.

◆ **TROUBLESHOOTING**

Post-processing quality control

● **TIMING 1 h**

30. To exclude gross artifacts and ensure the preservation of the expected structure in the expanded sample, it is good practice to conduct a comparative analysis of correlative pre- and post-expansion images. For this, images acquired in a few selected regions before expansion (Step 7) and ExSRRF reconstructions of the same sample areas are compared. Measuring representative distances and feature sizes in the image pairs also allows calculating the effective expansion factor.
31. Identifying processing artifacts and assessing processing performance
The computational detection of processing artifacts is performed based on super-resolution quality control algorithms. Based on the WF and super-resolved eSRRF image pair, NanoJ-SQUIRREL allows the calculation of an error map highlighting low-fidelity regions where reconstruction artifacts have been created by the processing (Plugins > NanoJ-SQUIRREL > Calculate Error-Map, RSE and RSP) (Fig. 4a–c). The achieved resolution enhancement should be assessed with the ImageJ Decorrelation Analysis plugin (https://github.com/Ades91/ImDecorr) by processing both the WF and the eSRRF reconstruction (Fig. 4d,e). Local changes in resolution are mapped based on FRC with NanoJ-SQUIRREL. For this, two independent eSRRF reconstructions of the same region are required. To generate this independent reconstruction, split the raw data into even and odd frames (Plugins > NanoJ-SQUIRREL > Tools > Split sequence into odd and even frames) and process both with the desired eSRRF parameters. Based on an image stack containing both reconstructions the FRC map is calculated (Plugins > NanoJ-SQUIRREL > Calculate FRC-Map) (Fig. 4f).
The same procedure can also be performed with NanoPyx Jupyter notebooks (https://github.com/HenriquesLab/NanoPyx/blob/main/notebooks/SRMetrics.ipynb). A step-by-step guide with examples can be found in the training manual (https://doi.org/10.5281/zenodo.11518140)[67].

Image analysis

32. Depending on the context and the target of the experiment, it may be of interest to identify fine ridge-like structures in the processed images, for example, membranes of cell organelles, vessel networks or the renal slit diaphragm. This can be accomplished with a multistep computational approach that leverages the scikit-image software package[68].
Briefly, the computational analysis consists of the following steps:
    - The ROI, that is, the portion of the image containing the target structure, should be identified and isolated either through manual cropping of the image or through automatic image processing. A Jupyter notebook with Python code to extract the ROI from an endoplasmic reticulum-specific staining is available through GitHub at https://github.com/imsb-uke/exsrrf_analyses/blob/main/ridges_er_stress.ipynb
    - Following restriction to the ROI, ridge-like structures can be identified through the use of ridge detection filters contained in the scikit-image software package[68], including filters based on the algorithms described by Meijering[69], Sato[70] and Frangi[71]. Ridge identification may be improved by thresholding the filter output, restricting the range of admissible object sizes to match the expected biological structures, and applying morphological operations, for example, opening, closing, dilation or erosion, to correct for imprecisions in the segmentation

- Based on ridge detection, several possible quantifications can be computed, including the density of the target structure, either globally within the ROI, within a given area or in the neighborhood of each pixel using a sliding window approach. Furthermore, the Euclidean distance transform can be employed to calculate the distance to the nearest ridge for all background pixels to identify areas with high inter-ridge spacing. Similarly, examining the distribution of the local densities and the distance to the nearest ridge provides a measure for the spatial uniformity of the structure of interest. A Jupyter notebook with exemplary Python code can be accessed at https://doi.org/10.5281/zenodo.11518140 (ref. 67)

Troubleshooting

Troubleshooting information can be found in Table 1

Table 1 | Troubleshooting table

Step	Problem	Possible reason	Solution
7	Slide scanning and stitching is not possible	The microscope does not have a slide scanning and stitching function	Manually scan the entire section at a reasonable resolution with overlapping edges, then use a third-party tool for image alignment Several computational open-source tools exist for the alignment of multitile image datasets for different platforms. Examples include 'BigStitcher' (Fiji based) and 'multiview-stitcher' (Python based/Napari). Detailed information regarding instructions and support can be found on the respective GitHub pages https://imagej.net/plugins/bigstitcher/ https://github.com/multiview-stitcher/napari-stitcher?tab=readme-ov-file https://github.com/multiview-stitcher/multiview-stitcher
8	Coverslip does not detach	Nail polish and mounting medium firmly attach coverslip to slide	Repeat the incubation in xylene for a prolonged time period. Coverslips may become harder to remove after longer mounting times. For example, when using Prolong Gold as a mounting medium, removing the coverslip after 1–2 d of mounting may not require any xylene, but after a time of 4–6 weeks, a prolonged incubation in xylene may be necessary Use a razor blade to carefully remove the nail polish after xylene treatment Insert a razor blade on the edge of the coverslip to carefully mobilize the coverslip as much as possible, then repeat incubation in xylene. These steps can be repeated several times until the coverslip is completely detached
12	Gelling solution prematurely forms a solid hydrogel	Cold chain of the gelling solution was interrupted 4HT inhibitor solution was too old 4HT inhibitor solution concentration was too low	The gelation is a temperature-dependent reaction. Interruptions in the cold chain can initiate unintended gel polymerization resulting in premature gelation. Strictly prepare the gelling solution on ice. Consider pre-chilling the pipette tips by placing them at −20 °C to 4 °C ~30 min before use. Pre-chill the tissue slides by placing them at 4 °C ~30 min before adding the gelling solution. Limit all work at room temperature to a minimal amount of time (<5 min) Old or insufficient concentrations of the 4HT inhibitor solution can contribute to an accelerated polymerization. Prepare fresh 4HT solution Use a higher concentration of the 4HT solution (i.e., 1.5× amount). When using higher concentrations of 4HT solution, longer polymerization times may be required[62]
13	Spacers slide inward	Spacers start to float in gelling solution	If spacers slide inward use forceps to re-adjust the spacers, then apply slight pressure to reinforce their position. Make sure to carefully assess the correct position of the gelling chamber spacers before starting polymerization step. Displacement of the spacers with superimposition onto the tissue section causes insufficient gel thickness, leads to gel instability and therefore interferes with tissue expansion An alternative solution to this problem could be to carefully attach the spacers to the slide using superglue, thereby preventing movement of the spacers. This strategy could safely immobilize the spacers, preventing them from sliding inward but has the downside that the spacers may be more difficult to remove, making the disassembly of the gelling chamber (Step 16) more challenging
13	Air bubbles trapped inside gelling chamber	Air bubbles are not in direct contact with the sample Air bubbles are in direct contact with the sample	No action needed. Air bubbles that are not in direct contact with the sample can be ignored as they do not interfere with the formation of the tissue–hydrogel hybrid Air bubbles that are in direct contact with the sample will interfere with the formation of the tissue–hydrogel hybrid and result in loss of tissue section in the area of the bubble. Move air bubbles sideways by either gently moving the top coverslip, gently pressing on top of the coverslip using laboratory forceps, forcing the air bubble to move laterally, or carefully adding activated gelling solution from one side of the gelling chamber If these steps fail to work, carefully remove the top coverslip, add new gelling solution and reassemble the gelling chamber by adding the top coverslip without introducing bubbles

Table 1 (continued) | Troubleshooting table

Step	Problem	Possible reason	Solution
14	Incomplete gel polymerization	Degraded gelling solution Insufficient sodium acrylate quality	If it is suspected that the gelling solution aliquot may have been degraded, thaw and use a new aliquot of gelling solution If this fails, preparing a new batch of gelling solution can be a useful next step. In our experience, the expansion method used in this paper is robust. While we have successfully used gelling stock solution that was stored at 4 °C for prolonged periods (i.e., several months) we do not recommend this procedure as we noted artifacts and reduced gel stability after prolonged periods of storage at 4 °C We therefore recommend storing the gelling stock solution at −20 °C for 1–6 months and thawing a fresh aliquot for each experiment Before preparing a new batch of gelling stock solution, the sodium acrylate quality should be assessed by making a sodium acrylate stock solution (38 g/100 ml) and examining the color[62]. The stock solution should be fully transparent and colorless. If a yellow tint is noted, discard the sodium acrylate batch and do not use it for the preparation of the gelling solution
16	Top coverslip breaks during gelling chamber disassembly	Top coverslip is lifted too quickly	If the top coverslip breaks, remove the broken part, dispose of in a suitable container and carefully start the process of coverslip removal from the opposing side. In general, use as little force and work as slowly as possible when deconstructing the gelling chamber to avoid breakage of the coverslips
20	Gel expands inhomogeneously	Insufficient homogenization	When using an alternative homogenization method (i.e., thermal homogenization) consider switching to a more potent homogenization such as proteinase K-based digestion as described in this protocol When encountering signs of insufficient digestion using proteinase K as described in this protocol, use a new aliquot or batch of proteinase K If problems still persist, consider increasing the proteinase K concentration, i.e., from 8 U/ml to 12 U/ml If problems still persist and proteinase K batch effects are ruled out, variations of the digestion buffer to enable higher proteinase K stability buffer by eliminating EDTA and providing a higher Ca^{2+} concentration have been described[12,41]: 50 mM TRIS, 800 mM guanidine HCl, 2 mM $CaCl_2$ and 0.5% (vol/vol) Triton X-100 in ddH_2O, with the pH adjusted to 8.0
20	Gel is sucked into the pipette	Direct contact of the hydrogel with the pipette tip of a pipette that creates a strong negative pressure	Avoid direct contact of the hydrogel with the pipette tip Additionally, use pipettes with a low negative pressure such as Pasteur pipettes or electrical/serological pipettes at the lowest settings. Pipettes that create a strong negative pressure (particularly 1,000 µl pipettes) can easily suck in the hydrogel into the pipette tip and destroy it upon direct contact. This is complicated by the fact that expanded hydrogels in ddH_2O are hard to see due to their high transparency. We therefore recommend using alternative pipettes with lower negative pressures and to work slowly. In addition, the pipette tip should face the bottom or the lateral wall of the well when removing ddH_2O to further reduce the risk of damaging the hydrogel
23	Sample cannot be located under the microscope	Sample flipped in the *z* axis	Carefully unmount the sample, rotate 180° in the *z* axis and remount with the help of a paintbrush and aluminum foil. During the expansion process samples can accidentally flip 180° in the *z* axis. Imaging of flipped samples may be impossible if the gel thickness exceeds the working distance of the objective and overall yield suboptimal imaging results
23	Gross tissue artifacts (i.e., ruptures, breakages, tears or distortions)	Overfixation using a crosslinking agent Problems with anchoring treatment Problems with polymer network Insufficient homogenization Rough sample handling	Use less harsh crosslinking agent for fixation (i.e., PFA instead of glutaraldehyde). If overfixation is assumed, use less strong PFA fixation. Consider using a non-crosslinking fixation agent (i.e., methanol) Use new aliquot of acryloyl-X. Consider changing the pH from neutral (7.4) to more alkaline (i.e., pH 10) to enhance NHS reactivity Consider switching to an alternative anchoring agent (i.e., MA-NHS) Consider using a fresh aliquot or prepare fresh gelling solution. Check sodium acrylate quality Avoid multiple freeze–thaw cycles of PrK aliquots. Consider optimizing PrK buffer (increased concentration of Ca^{2+} in the buffer may enhance the PrK activity). This can be achieved by lowering the EDTA content of the buffer[41]. Consider changing to a new batch of PrK Carefully avoid rough sample handling
24	Poor or no fluorescence signal	Poor labeling quality Fluorophore degradation	Carefully check the pre-expansion imaging signal to confirm labeling specificity and fidelity Validate that the fluorophores used in the experiment are compatible with the expansion process. Refer to Supplementary Table 1 for further information on the compatibility of fluorescent dyes, probes and proteins
24	Signal drops or is lost during acquisition	Photobleaching	Minimize exposure of samples to room light and avoid overexposure to high levels of microscope illumination during *z*-axis localization and sample imaging (reduce number of frames and illumination power) In the case of 3D imaging, the sample is exposed for the full duration of the *z*-stack acquisition, leading to an accumulation of photobleaching. If a loss of sample signal is visible across the *z*-stack, reduce the number of images acquired in each *z*-plane and the illumination power If photobleaching can not be sufficiently counteracted by adjusting the acquisition parameters, a fluoroprotective additive to the mounting media can be considered. Additives, such as sucrose, will reduce photobleaching while also leading to ~10% gel shrinkage[72]. Supplementary Fig. 3 demonstrates the effects of photobleaching, and the respective practice dataset can be found at https://doi.org/10.5281/zenodo.11518140 (ref. 67)

Table 1 (continued) | Troubleshooting table

Step	Problem	Possible reason	Solution
24	Movements during image acquisition	Excess water around the expanded sample in imaging chamber Insufficient coating of the imaging chamber Temperature variations Hydrogel shrinkage due to sample dehydration External sources of vibration	Carefully remove excess water around the expanded sample in imaging chamber using laboratory paper to minimize lateral movement Coat imaging chambers with poly-D-lysine. Overused poly-D-lysine can yield suboptimal results. In addition, the effect of poly-D-lysine coating fades away over time so ensure that the slides have been coated no more than a few days in advance Equilibrate sample to the system and room temperature as changes in temperature can cause micromovements within the expanded hydrogel Keep samples hydrated by carefully applying a few drops of deionized water on top of the specimen to avoid shrinkage of hydrogels, especially during longer image acquisitions Minimize external sources of vibration such as opening and closing of doors to the room as much as possible
29	Achieved resolution is insufficient	Optical aberrations due to refractive index mismatch No sufficient fluorescent fluctuations observed Blurring due to movement artifacts	A mismatch in refractive index can cause spherical aberrations when imaging deep within a sample, reducing image quality. To prevent this, use a water-immersion objective or adjust the refractive index of the gel to match that required for an oil-immersion objective. One way to do this is by adding sucrose to the gel, as suggested by Gao et al.[72]. However, note that this adjustment may slightly reduce the gel's expansion factor Fluctuation frequency might not to be picked up due to long exposure time. Reduce the exposure time, if possible Consider using a fluorescent marker exhibiting a higher degree of fluctuations If blurring due to movement artifacts cannot be sufficiently corrected by applying vibration correction during eSRRF analysis or drift correction in a pre-processing step, minimize vibrations and drift by making sure the microscope and sample are well isolated, avoiding mechanical tensions in the sample holder and equilibrating thermal gradients before imaging
29	Very long processing times	Very large images Frame window too long Magnification is set too high Computation not speed optimized	Reduce the image size by cropping out empty areas or cutting the image down to relevant regions of interest Reduce the number of frames for eSRRF reconstruction if possible. In the eSRRF parameter sweep, it is also possible to test eSRRF performance for different frame windows and identify the minimum number of frames required for optimal reconstruction results If it is possible, reduce the magnification parameter Run on hardware that allows to take advantage of GPU acceleration and make sure to use the fastest processing unit in the eSRRF advanced settings

Timing

Completing all stages of the ExSRRF protocol requires ~3–4 d in total and involves ~7–9 h of bench, imaging and processing time. However, it has to be noted that, in particular, the imaging and processing time can be highly variable depending on sample size, experimental setup and question, image acquisition speed of the microscopy system, hardware-based computational processing speed and degree of automatization. Of note, the preparation of some stages/steps can be performed in parallel to optimize time management that we have highlighted within the protocol. In addition, the pre-expansion immunostaining and imaging can be done several days or weeks in advance, which could further facilitate time management.

Steps 1–6, molecular labeling of specimen: can be performed overnight and require ~4 h of bench time

Step 7, pre-expansion imaging: requires ~1 h of imaging time depending on sample size

Steps 8–9, anchoring: can be performed overnight and requires ~15 min of bench time

Steps 10–14, polymerization: requires ~3 h and 30 min of bench time

Steps 15–18, digestion: requires ~4.5 h and 30 min of bench time

Steps 19–20, expansion: requires ~1.5 h and 30 min of bench time

Steps 21–22, sample mounting: requires ~30 min and 15 min of bench time

Steps 23–24, post-expansion imaging: requires ~1 h but can be highly variable depending on sample size and overall experimental design

Steps 25–32, pre-processing quality control, computational image enhancement post-processing quality control and image analysis: requires ~1–2 h but can be variable depending on sample size, degree of automatization and overall experimental design

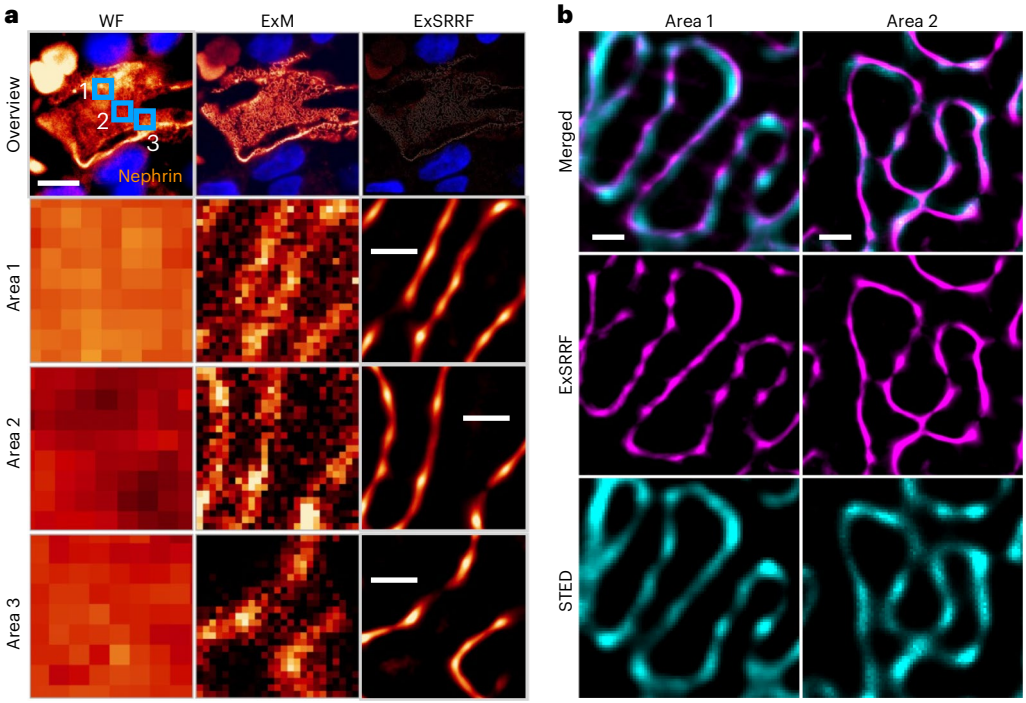

Fig. 5 | Anticipated results. a, Stepwise increase in resolution from WF to ExM to ExSRRF in human kidney tissue stained with nephrin to resolve the kidney slit diaphragm. Scale bar in the overview image, 5 µm, scale bars in the areas, 70 nm. **b**, Comparison between ExSRRF and STED in human kidney tissue stained with nephrin. Scale bars, 100 nm. Figure adapted from ref. 40 under a Creative Commons license CC BY 4.0 (https://creativecommons.org/licenses/by/4.0/).

Anticipated results

By following all steps in the protocol carefully, after a fourfold isotropic expansion of biological samples followed by fluorescence fluctuation analysis, a final resolution in the scale of 25 nm can be achieved in combination with diffraction-limited microscopes such as WF[40] and confocal[37] while maintaining the sample architecture and minimizing overall artifacts such as breaks, ruptures, distortions and reconstruction artifacts. The stepwise increase in resolution from diffraction-limited microscopy to ExM to the combined approach described in this paper as well as the overall expected data quality when imaging tissues using expansion and fluctuations enhancement of conventional LED-based epifluorescence microscopes is illustrated in Fig. 5. Here, the renal slit diaphragm is comparatively visualized with diffraction-limited microscopy, ExM and combined expansion and fluctuations enhancement. While diffraction-limited microscopy fails to provide adequate resolution to resolve the renal slit diaphragm, ExM already provides a resolution improvement for structures such as the slit diaphragm that cannot be resolved using conventional diffraction-limited microscopy. Ultimately, the combined expansion and fluctuations-enhancement approach (ExSRRF) further enhances the resolution, significantly contributing to a clearer view of the structure (Fig. 5a), delivering visual results comparable to advanced SRM techniques such as STED (Fig. 5b). Additional examples to further showcase the resolution range are demonstrated in Supplementary Fig. 4.

A visualization of artifacts that may be encountered is displayed in Fig. 2. Given the modular approach of this combined expansion and fluctuations-enhancement approach, artifacts due to tissue expansion as well as due to fluorescence fluctuation analysis can arise. Commonly encountered artifacts in ExM include the introduction of ruptures and breaks within the sample (Fig. 2a,b), which are further discussed within the troubleshooting section of the manuscript.

Besides rough tissue handling that may introduce artifacts, it is important to recognize that suboptimal anchoring and digestion processes are important sources of expansion-related artifacts and that these steps rely on chemical reactions that never achieve perfect efficiency. This is especially important in the context of a large variety of different biological sample types. For example, it is to be expected that a rigid FFPE clinical pathology sample may chemically and mechanically react differently than a single layer of fixed cells.

Besides expansion-induced artifacts, another important cause is sample movements during timelapse image acquisition that interfere with the fluorescence fluctuation detection (Fig. 2e). In our opinion, the best strategy here is to avoid lateral sample movements by optimizing the mounting and imaging conditions as discussed in the troubleshooting section. In case sample movements cannot be avoided, we recommend computational recovery of sample drifts before or during fluorescence fluctuation processing (Fig. 2c–f). Based on our experience, when mounting was performed as described here, sample drifts are rare and computational recovery, if required, is generally successful[40], making expansion and fluctuations-enhanced microscopy a robust, powerful, and flexible microscopy tool in life sciences to enhance the resolution of diffraction-limited microscopes, which has recently increasingly been recognized by the scientific community[14,36,37,40].

Reporting summary

Further information on research design is available in the Nature Portfolio Reporting Summary linked to this article.

Data availability

The main datasets were published in the original publication[40]. Test datasets are available via Zenodo at https://doi.org/10.5281/zenodo.11518140 (ref. 67).

Code availability

The code used and described in this paper is available via Zenodo at https://doi.org/10.5281/zenodo.11518140 (ref. 67) and GitHub at https://github.com/HenriquesLab/NanoJ-eSRRF and https://github.com/HenriquesLab/Nanopyx. Additional advice on how to use it can be obtained from the corresponding authors upon reasonable request. A Jupyter notebook with Python code to extract the ROI from an endoplasmic reticulum-specific staining is available through GitHub at https://github.com/imsb-uke/exsrrf_analyses/blob/main/ridges_er_stress.ipynb. A Jupyter notebook with exemplary Python code can be accessed via Zenodo at https://doi.org/10.5281/zenodo.11518140 (ref. 67).

Received: 7 July 2024; Accepted: 19 March 2025;
Published online: 02 July 2025

References

1. Gustafsson, M. G. L. Surpassing the lateral resolution limit by a factor of two using structured illumination microscopy. *J. Microsc.* **198**, 82–87 (2000).
2. Gustafsson, M. G. L. Nonlinear structured-illumination microscopy: wide-field fluorescence imaging with theoretically unlimited resolution. *Proc. Natl Acad. Sci. USA* **102**, 13081–13086 (2005).
3. Hell, S. W. & Wichmann, J. Breaking the diffraction resolution limit by stimulated emission: stimulated-emission-depletion fluorescence microscopy. *Opt. Lett.* **19**, 780 (1994).
4. Betzig, E. et al. Imaging intracellular fluorescent proteins at nanometer resolution. *Science* **313**, 1642–1645 (2006).
5. Rust, M. J., Bates, M. & Zhuang, X. Sub-diffraction-limit imaging by stochastic optical reconstruction microscopy (STORM). *Nat. Methods* **3**, 793–796 (2006).
6. Heilemann, M. et al. Subdiffraction-resolution fluorescence imaging with conventional fluorescent probes. *Angew. Chem. Int. Ed.* **47**, 6172–6176 (2008).
7. Bond, C., Santiago-Ruiz, A. N., Tang, Q. & Lakadamyali, M. Technological advances in super-resolution microscopy to study cellular processes. *Mol. Cell* **82**, 315–332 (2022).
8. Chen, F., Tillberg, P. W. & Boyden, E. S. Expansion microscopy. *Science* **347**, 543–548 (2015).
9. Tillberg, P. W. et al. Protein-retention expansion microscopy of cells and tissues labeled using standard fluorescent proteins and antibodies. *Nat. Biotechnol.* **34**, 987–992 (2016).
10. Zhao, Y. et al. Nanoscale imaging of clinical specimens using pathology-optimized expansion microscopy. *Nat. Biotechnol.* **35**, 757–764 (2017).
11. Chang, J.-B. et al. Iterative expansion microscopy. *Nat. Methods* **14**, 593–599 (2017).
12. Truckenbrodt, S. et al. X10 expansion microscopy enables 25-nm resolution on conventional microscopes. *EMBO Rep.* **19**, e45836 (2018).
13. Damstra, H. G. et al. Visualizing cellular and tissue ultrastructure using ten-fold robust expansion microscopy (TREx). *eLife* **11**, e73775 (2022).
14. Klimas, A. et al. Magnify is a universal molecular anchoring strategy for expansion microscopy. *Nat. Biotechnol.* **41**, 858–869 (2023).
15. Gao, R. et al. Cortical column and whole-brain imaging with molecular contrast and nanoscale resolution. *Science* **363**, eaau8302 (2019).

16. Suen, K. M. et al. Expansion microscopy reveals subdomains in *C. elegans* germ granules. *Life Sci. Alliance* **6**, e202201650 (2023).
17. Pownall, M. E. et al. Chromatin expansion microscopy reveals nanoscale organization of transcription and chromatin. *Science* **381**, 92–100 (2023).
18. Sarkar, D. et al. Revealing nanostructures in brain tissue via protein decrowding by iterative expansion microscopy. *Nat. Biomed. Eng.* **6**, 1057–1073 (2022).
19. Wen, G., Leen, V., Rohand, T., Sauer, M. & Hofkens, J. Current progress in expansion microscopy: chemical strategies and applications. *Chem. Rev.* **123**, 3299–3323 (2023).
20. Sun, D. et al. Click-ExM enables expansion microscopy for all biomolecules. *Nat. Methods* **18**, 107–113 (2021).
21. Chen, F. et al. Nanoscale imaging of RNA with expansion microscopy. *Nat. Methods* **13**, 679–684 (2016).
22. Gambarotto, D. et al. Imaging cellular ultrastructures using expansion microscopy (U-ExM). *Nat. Methods* **16**, 71–74 (2019).
23. Louvel, V. et al. iU-ExM: nanoscopy of organelles and tissues with iterative ultrastructure expansion microscopy. *Nat. Commun.* **14**, 7893 (2023).
24. M'Saad, O. & Bewersdorf, J. Light microscopy of proteins in their ultrastructural context. *Nat. Commun.* **11**, 3850 (2020).
25. Ku, T. et al. Multiplexed and scalable super-resolution imaging of three-dimensional protein localization in size-adjustable tissues. *Nat. Biotechnol.* **34**, 973–981 (2016).
26. Dertinger, T., Colyer, R., Iyer, G., Weiss, S. & Enderlein, J. Fast, background-free, 3D super-resolution optical fluctuation imaging (SOFI). *Proc. Natl Acad. Sci. USA* **106**, 22287–22292 (2009).
27. Cox, S. et al. Bayesian localization microscopy reveals nanoscale podosome dynamics. *Nat. Methods* **9**, 195–200 (2012).
28. Agarwal, K. & Macháň, R. Multiple signal classification algorithm for super-resolution fluorescence microscopy. *Nat. Commun.* **7**, 13752 (2016).
29. Zhao, W., Liu, J. & Li, H. Ultrafast super-resolution imaging via auto-correlation two-step deconvolution. In *Ultrafast Nonlinear Imaging and Spectroscopy VIII* (eds Liu, Z., Psaltis, D. & Shi, K.) 29 (SPIE, 2020); https://doi.org/10.1117/12.2567853
30. Gustafsson, N. et al. Fast live-cell conventional fluorophore nanoscopy with ImageJ through super-resolution radial fluctuations. *Nat. Commun.* **7**, 12471 (2016).
31. Laine, R. F. et al. High-fidelity 3D live-cell nanoscopy through data-driven enhanced super-resolution radial fluctuation. *Nat. Methods* **20**, 1949–1956 (2023).
32. Stubb, A. et al. Fluctuation-based super-resolution traction force microscopy. *Nano Lett.* **20**, 2230–2245 (2020).
33. Grant, S. D., Cairns, G. S., Wistuba, J. & Patton, B. R. Adapting the 3D-printed Openflexure microscope enables computational super-resolution imaging. *F1000Res* **8**, 2003 (2019).
34. Dey, G. et al. Closed mitosis requires local disassembly of the nuclear envelope. *Nature* **585**, 119–123 (2020).
35. Ecke, M. et al. Formins specify membrane patterns generated by propagating actin waves. *Mol. Biol. Cell* **31**, 373–385 (2020).
36. Shaib, A. H. et al. One-step nanoscale expansion microscopy reveals individual protein shapes. *Nat. Biotechnol.* https://doi.org/10.1038/s41587-024-02431-9 (2024).
37. Wang, B. et al. Multicomposite super-resolution microscopy: enhanced airyscan resolution with radial fluctuation and sample expansions. *J. Biophoton.* **13**, e2419 (2020).
38. Zeng, Z., Ma, J. & Xu, C. Cross-cumulant enhanced radiality nanoscopy for multicolor superresolution subcellular imaging. *Photon. Res.* **8**, 893–898 (2020).
39. Culley, S., Tosheva, K. L., Matos Pereira, P. & Henriques, R. SRRF: universal live-cell super-resolution microscopy. *Int. J. Biochem. Cell Biol.* **101**, 74–79 (2018).
40. Kylies, D. et al. Expansion-enhanced super-resolution radial fluctuations enable nanoscale molecular profiling of pathology specimens. *Nat. Nanotechnol.* **18**, 336–342 (2023).
41. Truckenbrodt, S., Sommer, C., Rizzoli, S. O. & Danzl, J. G. A practical guide to optimization in X10 expansion microscopy. *Nat. Protoc.* **14**, 832–863 (2019).
42. Lee, M. Y. et al. Fluorescent labeling of abundant reactive entities (FLARE) for cleared-tissue and super-resolution microscopy. *Nat. Protoc.* **17**, 819–846 (2022).
43. Wang, Y. et al. Combined expansion microscopy with structured illumination microscopy for analyzing protein complexes. *Nat. Protoc.* **13**, 1869–1895 (2018).
44. Bucur, O. et al. Nanoscale imaging of clinical specimens using conventional and rapid-expansion pathology. *Nat. Protoc.* **15**, 1649–1672 (2020).
45. Culley, S. et al. Quantitative mapping and minimization of super-resolution optical imaging artifacts. *Nat. Methods* **15**, 263–266 (2018).
46. Opstad, I. S. et al. Fluorescence fluctuations-based super-resolution microscopy techniques: an experimental comparative study. Preprint at http://arxiv.org/abs/2008.09195 (2020).
47. Valli, J. et al. Seeing beyond the limit: a guide to choosing the right super-resolution microscopy technique. *J. Biol. Chem.* **297**, 100791 (2021).
48. Zwettler, F. U. et al. Molecular resolution imaging by post-labeling expansion single-molecule localization microscopy (Ex-SMLM). *Nat. Commun.* **11**, 3388 (2020).
49. Saal, K. A. et al. Heat denaturation enables multicolor X10-STED microscopy. *Sci. Rep.* **13**, 5366 (2023).
50. Mikhaylova, M. et al. Resolving bundled microtubules using anti-tubulin nanobodies. *Nat. Commun.* **6**, 7933 (2015).
51. Shi, X. et al. Label-retention expansion microscopy. *J. Cell Biol.* **220**, e202105067 (2021).
52. Wen, G. et al. Evaluation of direct grafting strategies via trivalent anchoring for enabling lipid membrane and cytoskeleton staining in expansion microscopy. *ACS Nano* **14**, 7860–7867 (2020).
53. Lukinavičius, G. et al. Fluorogenic probes for live-cell imaging of the cytoskeleton. *Nat. Methods* **11**, 731–733 (2014).
54. Helmerich, D. A., Beliu, G. & Sauer, M. Multiple-labeled antibodies behave like single emitters in photoswitching buffer. *ACS Nano* **14**, 12629–12641 (2020).
55. Steib, E. et al. TissUExM enables quantitative ultrastructural analysis in whole vertebrate embryos by expansion microscopy. *Cell Rep. Methods* **2**, 100311 (2022).
56. Sim, J. et al. Nanoscale resolution imaging of whole mouse embryos using expansion microscopy. *ACS Nano* **19**, 7910-7927 (2025).
57. Wang, M. & Wang, W.-X. Nanoscale whole-body expansion microscopy revealed the early skeletal developmental malformation induced by silver nanoparticles. *Environ. Sci. Technol. Lett.* **10**, 471–477 (2023).
58. Wassie, A. T., Zhao, Y. & Boyden, E. S. Expansion microscopy: principles and uses in biological research. *Nat. Methods* **16**, 33–41 (2019).
59. Scandella, V., Paolicelli, R. C. & Knobloch, M. A novel protocol to detect green fluorescent protein in unfixed, snap-frozen tissue. *Sci. Rep.* **10**, 14642 (2020).
60. Bokman, S. H. & Ward, W. W. Renaturation of Aequorea green-fluorescent protein. *Biochem. Biophys. Res. Commun.* **101**, 1372–1380 (1981).
61. Sniegowski, J. A., Phail, M. E. & Wachter, R. M. Maturation efficiency, trypsin sensitivity, and optical properties of Arg96, Glu222, and Gly67 variants of green fluorescent protein. *Biochem. Biophys. Res. Commun.* **332**, 657–663 (2005).
62. Asano, S. M. et al. Expansion microscopy: protocols for imaging proteins and RNA in cells and tissues. *Curr. Protoc. Cell Biol.* **80**, e56 (2018).
63. Gao, R., Asano, S. M. & Boyden, E. S. Q&A: expansion microscopy. *BMC Biol.* **15**, 50 (2017).
64. Laine, R. F. et al. NanoJ: a high-performance open-source super-resolution microscopy toolbox. *J. Phys. D.* **52**, 163001 (2019).
65. Schindelin, J. et al. Fiji: an open-source platform for biological-image analysis. *Nat. Methods* **9**, 676–682 (2012).
66. Saraiva, B. M. et al. Efficiently accelerated bioimage analysis with NanoPyx, a Liquid Engine-powered Python framework. *Nat Methods* **22**, 283–286 (2025).
67. Kylies, D. et al. Expansion and fluctuations-enhanced microscopy for nanoscale molecular profiling of cells and tissues—data processing manual [Data set]. *Zenodo* https://doi.org/10.5281/zenodo.11518140 (2024).
68. Van Der Walt, S. et al. scikit-image: image processing in Python. *PeerJ* **2**, e453 (2014).
69. Meijering, E. et al. Design and validation of a tool for neurite tracing and analysis in fluorescence microscopy images. *Cytom. A* **58**, 167–176 (2004).
70. Sato, Y. et al. Three-dimensional multi-scale line filter for segmentation and visualization of curvilinear structures in medical images. *Med. Image Anal.* **2**, 143–168 (1998).
71. Frangi, A. F., Niessen, W. J., Vincken, K. L. & Viergever, M. A. Multiscale vessel enhancement filtering. In *Medical Image Computing and Computer-Assisted Intervention—MICCAI'98* Vol. 1496 (eds Wells, W. M., Colchester, A. & Delp, S.) 130–137 (Springer, 1998).
72. Gao, M. et al. Expansion stimulated emission depletion microscopy (ExSTED). *ACS Nano* **12**, 4178–4185 (2018).
73. Chozinski, T. J. et al. Expansion microscopy with conventional antibodies and fluorescent proteins. *Nat. Methods* **13**, 485–488 (2016).
74. Park, J. et al. Epitope-preserving magnified analysis of proteome (eMAP). *Sci. Adv.* **7**, eabf6589 (2021).
75. Heil, H. S. et al. Mapping densely packed αIIbβ3 receptors in murine blood platelets with expansion microscopy. *Platelets* **33**, 849–858 (2022).
76. Vanheusden, M. et al. Fluorescence photobleaching as an intrinsic tool to quantify the 3D expansion factor of biological samples in expansion microscopy. *ACS Omega* **5**, 6792–6799 (2020).
77. Scheible, M. B. & Tinnefeld, P. Quantifying expansion microscopy with DNA origami expansion nanorulers. Preprint at *bioRxiv* https://doi.org/10.1101/265405 (2018).
78. Damstra, H. G. J. et al. GelMap: intrinsic calibration and deformation mapping for expansion microscopy. *Nat. Methods* **20**, 1573–1580 (2023).
79. Pesce, L., Cozzolino, M., Lanzanò, L., Diaspro, A. & Bianchini, P. Measuring expansion from macro- to nanoscale using NPC as intrinsic reporter. *J. Biophoton.* **12**, e201900018 (2019).
80. Nieuwenhuizen, R. P. J. et al. Measuring image resolution in optical nanoscopy. *Nat. Methods* **10**, 557–562 (2013).
81. Descloux, A., Grußmayer, K. S. & Radenovic, A. Parameter-free image resolution estimation based on decorrelation analysis. *Nat. Methods* **16**, 918–924 (2019).

Acknowledgements

This work was supported by the following grants: (1) The German Research Foundation: CRC/1192 to V.G.P.; (2) German Federal Ministry of Education and Research: eMed Consortia Fibromap to V.G.P.; STOP-FSGS-01GM2202A to V.G.P.; (3) The Novo Nordisk Foundation (Young Investigator Award; NNF21OC0066381) to V.G.P.; (4) The Else-Kröner-Fresenius-Stiftung and the Eva Luise und Horst Köhler Stiftung (2019_KollegSE.04 RECORD) to D.K.; (5) The doctoral college 'innovative Promotionsförderung im Bereich translationale Entzündungsforschung' (iPRIME) of the Else-Kröner-Fresenius Foundation to M.K.; (6) Intramural funding Clinician Scientist program to D.K.; (7) the Gulbenkian Foundation (Fundação Calouste Gulbenkian, to H.S.H., A.G.V., M.D.R. and R.H.); (8) the European Research Council under the European Union's Horizon 2020 research and innovation program (grant agreement no. 101001332 to R.H.) and the European Commission through the Horizon Europe program (AI4LIFE project with grant agreement 101057970-AI4LIFE and RT-SuperES project with grant agreement 101099654-RT-SuperES to R.H.); funded by the European Union. Views and opinions expressed are, however, those of the authors only and do not necessarily reflect those of the European Union. Neither

the European Union nor the granting authority can be held responsible for them; (9) the European Molecular Biology Organization (EMBO-2020-IG-4734 to R.H.); (10) the Fundação para a Ciência e Tecnologia, Portugal (FCT fellowship CEECIND/01480/2021 to H.S.H. and Associate Laboratory LS4FUTURE (LA/P/0087/2020, DOI 10.54499/LA/P/0087/2020) to R.H.); (11) the Chan Zuckerberg Initiative Visual Proteomics Grant (vpi-0000000044 with https://doi.org/10.37921/743590vtudfp) and the Chan Zuckerberg Initiative Essential Open Source Software for Science (EOSS6-0000000260) to R.H.; (12) A.G.V. acknowledges the support by the European Union's Horizon 2020 research and innovation program under the Marie Sklodowska-Curie grant agreement no. 101180631 (https://doi.org/10.3030/101180631). Figure 1a and Box 1 figure were created with BioRender.com. ChatGPT was used to assist with stylistic improvements and linguistic corrections in the writing process of the originally submitted manuscript. However, no contributions to the content or to the scientific analysis were made using LLMs.

Author contributions

D.K. developed and documented the ExSRRF protocol. H.S.H. developed and documented the image processing and quality control protocol. D.K. and H.S.H. provided test datasets. D.K. and H.S.H. contributed equally as co-first authors. A.G.V. wrote the eSRRF training manual. M.D.R. contributed to the troubleshooting section. M.K. developed and tested Python notebooks for image analysis. M.S. and M.N.W. provided biological and technical expertise. All authors contributed to the writing of the paper. V.G.P. and R.H. jointly supervised the project.

Competing interests

The authors declare no competing interests.

Additional information

Extended data is available for this paper at https://doi.org/10.1038/s41596-025-01178-0.

Supplementary information The online version contains supplementary material available at https://doi.org/10.1038/s41596-025-01178-0.

Correspondence and requests for materials should be addressed to Victor G. Puelles or Ricardo Henriques.

Peer review information *Nature Protocols* thanks the anonymous reviewers for their contribution to the peer review of this work.

Reprints and permissions information is available at www.nature.com/reprints.

Publisher's note Springer Nature remains neutral with regard to jurisdictional claims in published maps and institutional affiliations.

[1]III. Department of Medicine, University Medical Center Hamburg–Eppendorf, Hamburg, Germany. [2]Hamburg Center for Kidney Health (HCKH), University Medical Center Hamburg-Eppendorf, Hamburg, Germany. [3]Optical Cell Biology, Instituto Gulbenkian de Ciência, Oeiras, Portugal. [4]Instituto de Tecnologia Química e Biológica António Xavier, Universidade Nova de Lisboa, Oeiras, Portugal. [5]Department of Clinical Medicine, Aarhus University, Aarhus, Denmark. [6]Department of Pathology, Aarhus University Hospital, Aarhus, Denmark. [7]Laboratory for Molecular Cell Biology, University College London, London, UK. [8]Present address: Department of Clinical Sciences, Faculty of Medicine, Lund University, Lund, Sweden. [9]These authors contributed equally: Dominik Kylies, Hannah S. Heil. [10]These authors jointly supervised this work: Victor G. Puelles, Ricardo Henriques.

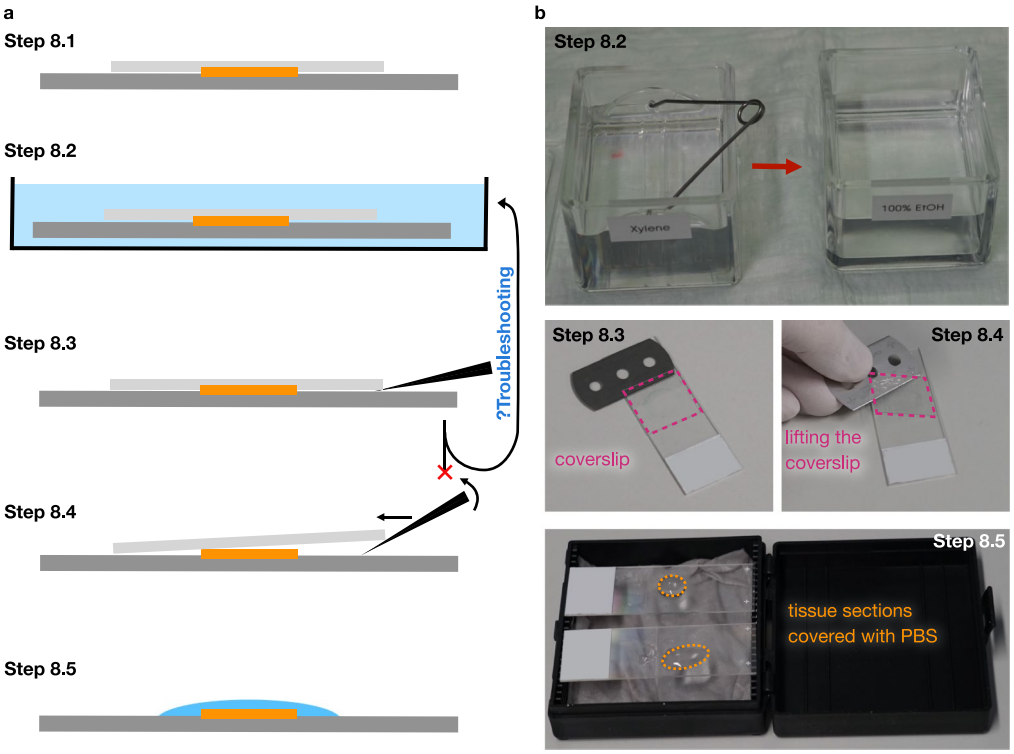

Extended Data Fig. 1 | Coverslip removal. a. Graphical explanation of coverslip removal. Stained and mounted sections (Step 8.1) are immersed in xylene followed by ethanol (Step 8.2) to remove nail polish and soften the mounting media to facilitate coverslip removal. Next, a razor blade is carefully inserted between the coverslip and slide at the edge of the coverslip (Step 8.3) and slowly angled and moved forward (Step 8.4) to separate the coverslip and slide. The remaining mounting media is washed off with PBS (Step 8.5). In case the coverslip can't be separated from the slide consult the instructions in the Troubleshooting table - Step 8, such as repeating the xylene incubation. **b.** Foto examples of the respective steps.

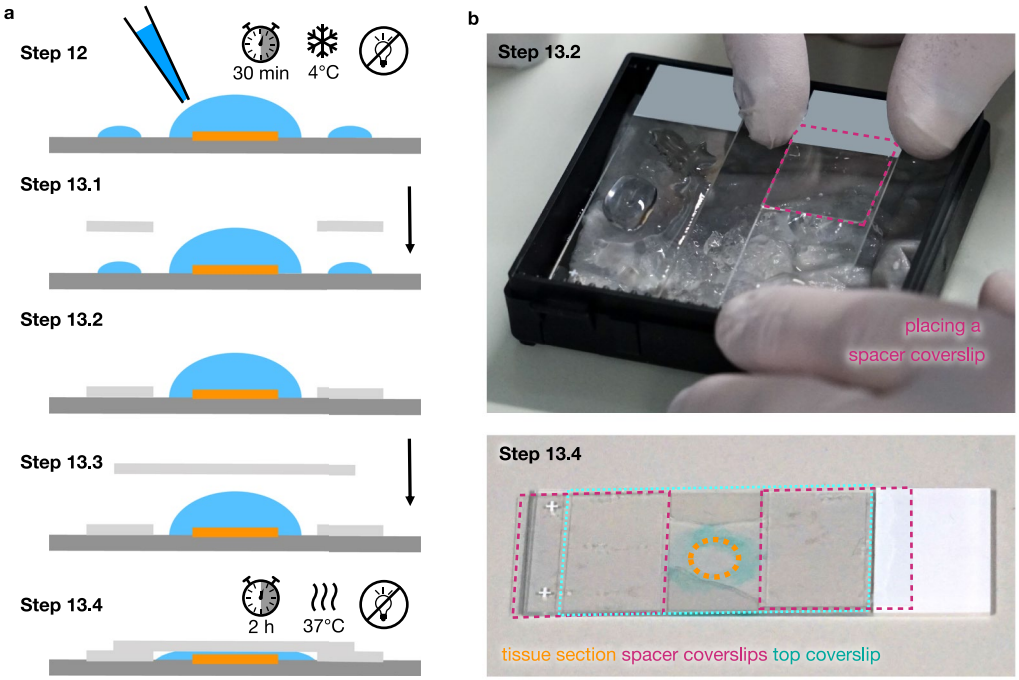

Extended Data Fig. 2 | Gelling solution penetration and assembly of the gelling chamber. a. Graphical explanation of the monomer penetration step and the gelling chamber assembly. Activated gelling solution is pipetted onto the tissue section to allow for penetration into the tissue section, as well as laterally of the tissue section to facilitate the attachment of the gelling chamber spacer glasses (Step 12). After completion of the incubation at 4°C, the gelling chamber is assembled by placing two coverslips as spacers laterally of the tissue section (Step 13.1, 13.2) followed by a third, larger coverglass on top of the tissue section and the spacers (Step 13.3) fully covering the tissue section and without introducing bubbles (Step 13.4). **b**. Foto examples of the critical steps.

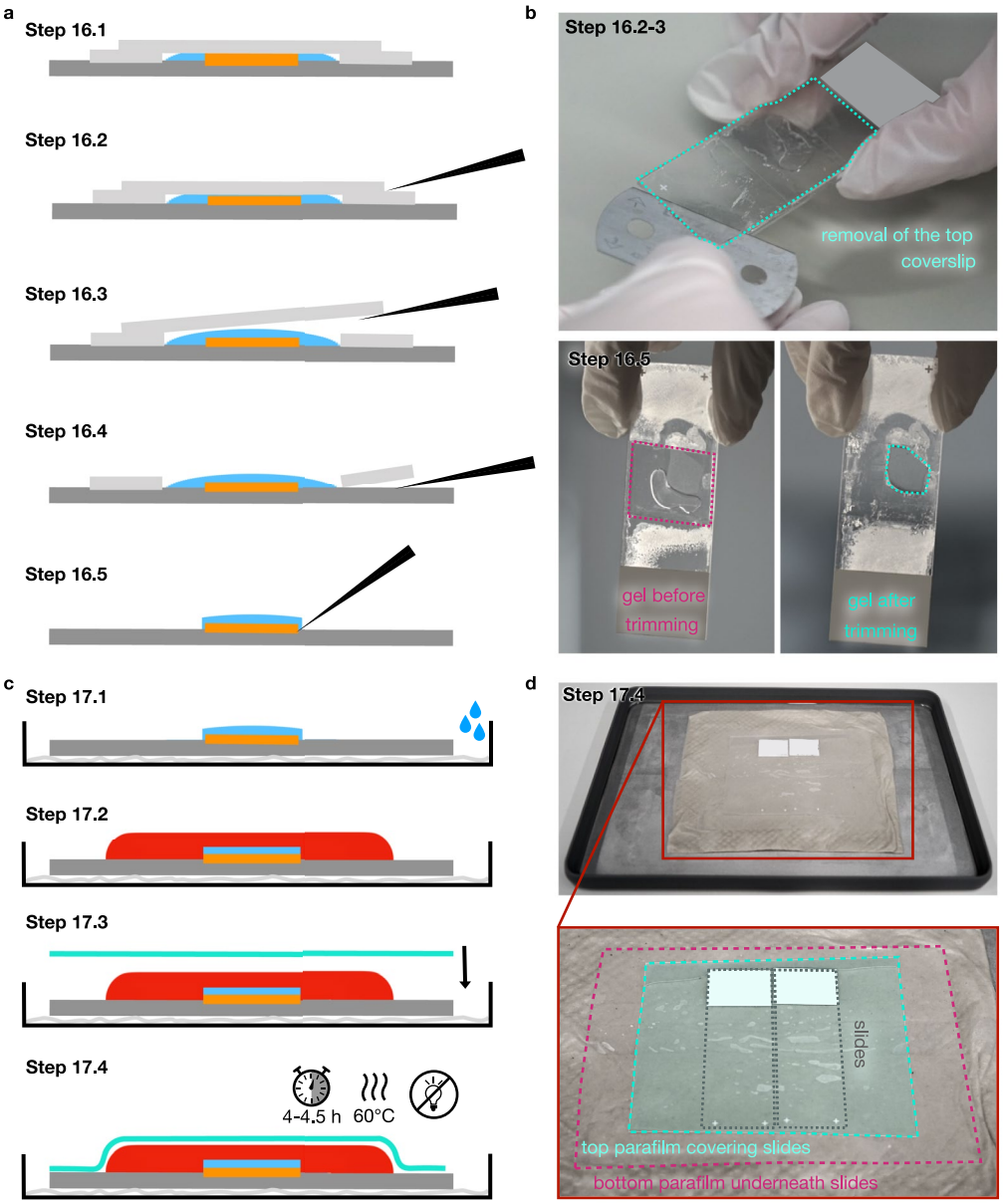

Extended Data Fig. 3 | Gelling chamber disassembly and digestion setup. **a**. Graphical explanation of the gelling chamber (Step 16.1) disassembly. Using a razor blade, the top coverslip (Step 16.2, 16.3), then the spacer coverslips (Step 16.4) are removed. Excess gel is trimmed from the slide (Step 16.5). **b**. Foto examples of the gelling chamber disassembly and of the tissue hydrogel hybrid before and after trimming. **c**. Graphical explanation of the digestion setup. After removal of the gelling chamber and hydrogel trimming, the slide is moved onto a tray (Step 17.1) containing a humidified paper and a bottom parafilm piece on top of the humidified paper to avoid leakage of digestion solution into the humidified paper. Next, the digestion solution (red) is pipetted onto the specimen (Step 17.2) after which a second piece of parafilm (cyan) is carefully placed on top of the specimen (Step 17.3, 17.4) without introducing bubbles between the parafilm and the specimen to prevent evaporation of the digestion solution during incubation. The specimen is then moved into the oven for incubation. **d**. Foto examples of the incubation setup.

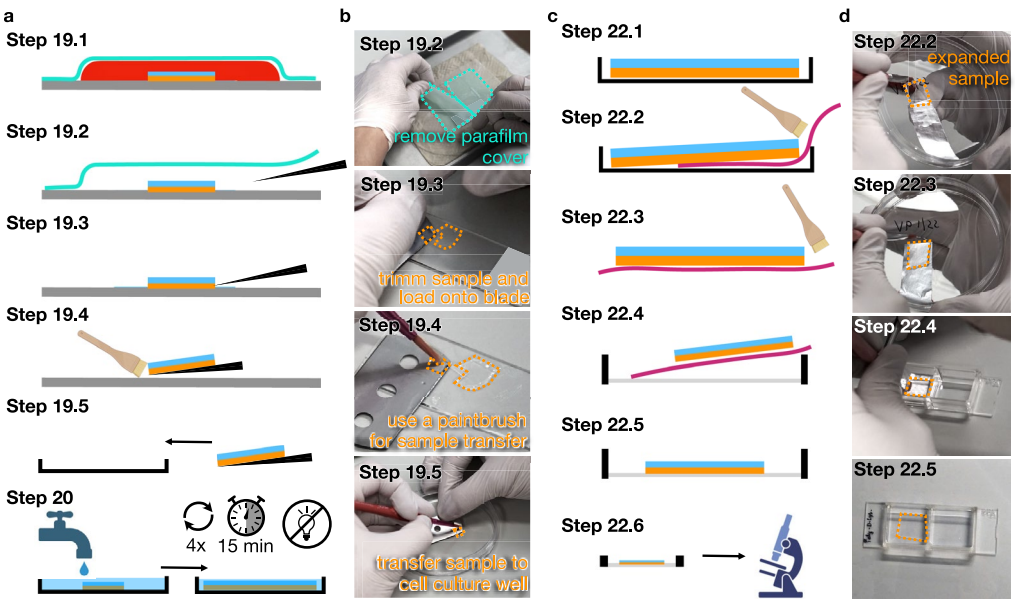

Extended Data Fig. 4 | Tissue expansion and sample mounting. a. Graphical explanation of tissue expansion stage. After samples are removed from the digestion incubator and have cooled off, they are placed on a clean work surface (Step 19.1) and the parafilm cover is removed using a razor blade (Step 19.2). Next, the sample is separated from the slide with the help of a razor blade (Step 19.3) and loaded onto the razor blade with the help of a paintbrush (Step 19.4) to transfer the sample to the cell culture well (Step 19.5). Tissue expansion is then performed by carefully adding ddH2O to the sample (Step 20). **b**. Foto examples of critical handling steps during the tissue expansion stage. Note that larger samples can also be trimmed on the slide (Step 19.3, 19.4). **c**. Graphical explanation of the sample mounting stage. Expanded specimens (Step 22.1) are loaded onto a piece of aluminum foil with the help of a paintbrush (Step 22.2) and transferred (Step 22.3) to the coated imaging chamber into which the samples are transferred by holding the sample in place with the paintbrush while carefully and slowly pulling out the aluminum foil from underneath the sample (Step 22.4). The mounted samples (Step 22.5) are then transferred to the microscope for imaging (Step 22.6). **d**. Foto examples of critical handling steps during the sample mounting stage.

nature portfolio

Corresponding author(s): Victor G. Puelles
Ricardo Henriques

Last updated by author(s): Feb 24, 2025

Reporting Summary

Nature Portfolio wishes to improve the reproducibility of the work that we publish. This form provides structure for consistency and transparency in reporting. For further information on Nature Portfolio policies, see our Editorial Policies and the Editorial Policy Checklist.

Statistics

For all statistical analyses, confirm that the following items are present in the figure legend, table legend, main text, or Methods section.

n/a	Confirmed	
☒	☐	The exact sample size (*n*) for each experimental group/condition, given as a discrete number and unit of measurement
☒	☐	A statement on whether measurements were taken from distinct samples or whether the same sample was measured repeatedly
☒	☐	The statistical test(s) used AND whether they are one- or two-sided *Only common tests should be described solely by name; describe more complex techniques in the Methods section.*
☒	☐	A description of all covariates tested
☒	☐	A description of any assumptions or corrections, such as tests of normality and adjustment for multiple comparisons
☒	☐	A full description of the statistical parameters including central tendency (e.g. means) or other basic estimates (e.g. regression coefficient) AND variation (e.g. standard deviation) or associated estimates of uncertainty (e.g. confidence intervals)
☒	☐	For null hypothesis testing, the test statistic (e.g. *F*, *t*, *r*) with confidence intervals, effect sizes, degrees of freedom and *P* value noted *Give P values as exact values whenever suitable.*
☒	☐	For Bayesian analysis, information on the choice of priors and Markov chain Monte Carlo settings
☒	☐	For hierarchical and complex designs, identification of the appropriate level for tests and full reporting of outcomes
☒	☐	Estimates of effect sizes (e.g. Cohen's *d*, Pearson's *r*), indicating how they were calculated

Our web collection on statistics for biologists contains articles on many of the points above.

Software and code

Policy information about availability of computer code

Data collection	n/a
Data analysis	n/a

For manuscripts utilizing custom algorithms or software that are central to the research but not yet described in published literature, software must be made available to editors and reviewers. We strongly encourage code deposition in a community repository (e.g. GitHub). See the Nature Portfolio guidelines for submitting code & software for further information.

Data

Policy information about availability of data

All manuscripts must include a data availability statement. This statement should provide the following information, where applicable:

- Accession codes, unique identifiers, or web links for publicly available datasets
- A description of any restrictions on data availability
- For clinical datasets or third party data, please ensure that the statement adheres to our policy

The main data sets were published in the original publication (Kylies et al. Nature Nanotechonolgy, 2023). Test datasets are available on Zenodo: https://zenodo.org/doi/10.5281/zenodo.11518140.

Research involving human participants, their data, or biological material

Policy information about studies with human participants or human data. See also policy information about sex, gender (identity/presentation), and sexual orientation and race, ethnicity and racism.

Reporting on sex and gender	n/a
Reporting on race, ethnicity, or other socially relevant groupings	n/a
Population characteristics	n/a
Recruitment	n/a
Ethics oversight	We exemplify our protocol using ExSRRF images from formalin-fixed paraffin-embedded (FFPE) kidney sections. The corresponding datasets and ethics approvals were published and described in the original publication (Kylies et al., Nature Nanotechnology, 2023)

Note that full information on the approval of the study protocol must also be provided in the manuscript.

Field-specific reporting

Please select the one below that is the best fit for your research. If you are not sure, read the appropriate sections before making your selection.

☒ Life sciences ☐ Behavioural & social sciences ☐ Ecological, evolutionary & environmental sciences

For a reference copy of the document with all sections, see nature.com/documents/nr-reporting-summary-flat.pdf

Life sciences study design

All studies must disclose on these points even when the disclosure is negative.

Sample size	n/a
Data exclusions	n/a
Replication	n/a
Randomization	n/a
Blinding	n/a

Reporting for specific materials, systems and methods

We require information from authors about some types of materials, experimental systems and methods used in many studies. Here, indicate whether each material, system or method listed is relevant to your study. If you are not sure if a list item applies to your research, read the appropriate section before selecting a response.

Materials & experimental systems

n/a	Involved in the study
☐	☒ Antibodies
☐	☒ Eukaryotic cell lines
☒	☐ Palaeontology and archaeology
☐	☒ Animals and other organisms
☒	☐ Clinical data
☒	☐ Dual use research of concern
☒	☐ Plants

Methods

n/a	Involved in the study
☒	☐ ChIP-seq
☒	☐ Flow cytometry
☒	☐ MRI-based neuroimaging

Antibodies

Antibodies used	A thorough description of all applicable antibodies are listed in the underlying primary publications of this manuscript: Kylies, et al. Nat. Nanotechnol. 18, 336–342 (2023). https://doi.org/10.1038/s41565-023-01328-z and Laine, Heil et al. Nat Methods 20, 1949–1956 (2023). https://doi.org/10.1038/s41592-023-02057-w

Validation	A thorough description the validations are listed in the underlying primary publications of this manuscript: Kylies, et al. Nat. Nanotechnol. 18, 336–342 (2023). https://doi.org/10.1038/s41565-023-01328-z and Laine, Heil et al. Nat Methods 20, 1949–1956 (2023). https://doi.org/10.1038/s41592-023-02057-w

Eukaryotic cell lines

Policy information about cell lines and Sex and Gender in Research

Cell line source(s)	As stated in the manuscript, a thorough description of the applicable cell lines is listed in one of the underlying primary publication of this manuscript: Laine, Heil et al. Nat Methods 20, 1949–1956 (2023). https://doi.org/10.1038/s41592-023-02057-w
Authentication	As stated in the manuscript, authentication of the applicable cell lines is listed in one of the underlying primary publication of this manuscript: Laine, Heil et al. Nat Methods 20, 1949–1956 (2023). https://doi.org/10.1038/s41592-023-02057-w
Mycoplasma contamination	All applicable information is disclosed in one of the underlying primary publication of this manuscript: Laine, Heil et al. Nat Methods 20, 1949–1956 (2023). https://doi.org/10.1038/s41592-023-02057-w
Commonly misidentified lines (See ICLAC register)	All applicable information is disclosed in one of the underlying primary publication of this manuscript: Laine, Heil et al. Nat Methods 20, 1949–1956 (2023). https://doi.org/10.1038/s41592-023-02057-w

Animals and other research organisms

Policy information about studies involving animals; ARRIVE guidelines recommended for reporting animal research, and Sex and Gender in Research

Laboratory animals	A thorough description of all laboratory animals is listed in one of the underlying primary publications of this manuscript: Kylies, et al. Nat. Nanotechnol. 18, 336–342 (2023). https://doi.org/10.1038/s41565-023-01328-z
Wild animals	n/a
Reporting on sex	n/a
Field-collected samples	n/a
Ethics oversight	A thorough description of applicable ethics on laboratory animals is listed in one of the underlying primary publications of this manuscript: Kylies, et al. Nat. Nanotechnol. 18, 336–342 (2023). https://doi.org/10.1038/s41565-023-01328-z

Note that full information on the approval of the study protocol must also be provided in the manuscript.

Plants

Seed stocks	n/a
Novel plant genotypes	n/a
Authentication	n/a